Accepted Manuscript

Design, synthesis, and biological evaluation of rutacecarpine derivatives as multitarget-directed ligands for the treatment of Alzheimer's disease

Mingfei Wu, Jie Ma, Lijun Ji, Min Wang, Jianfei Han, Zeng Li

PII: S0223-5234(19)30465-9

DOI: https://doi.org/10.1016/j.ejmech.2019.05.055

Reference: EJMECH 11365

To appear in: *European Journal of Medicinal Chemistry*

Received Date: 4 March 2019

Revised Date: 22 April 2019

Accepted Date: 19 May 2019

Please cite this article as: M. Wu, J. Ma, L. Ji, M. Wang, J. Han, Z. Li, Design, synthesis, and biological evaluation of rutacecarpine derivatives as multitarget-directed ligands for the treatment of Alzheimer's disease, *European Journal of Medicinal Chemistry* (2019), doi: https://doi.org/10.1016/j.ejmech.2019.05.055.

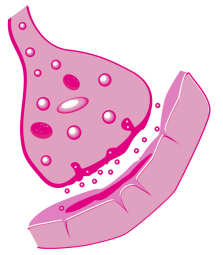

BuChE activity

IC_{50}: 3.60 ± 0.34 μM

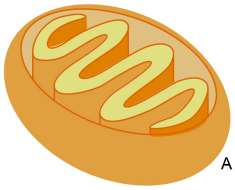

Scavenging ROS

A promising neuroantioxidant

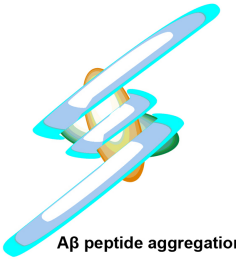

Aβ peptide aggregation inhibition

Self-mediated Aβ aggregation: 58.95%

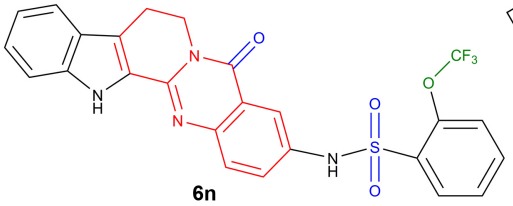

6n

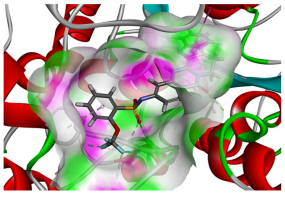

Docking analysis

Conventional hydrogen bond,

Carbon hydrogen bond, Halogen interaction

PC12 cell

SH-SY5Y cell

Neuroprotection study

Anti-H2O2 cytotoxicity,

Anti-Aβ cytotoxicity

Metal-chelating property

Selectivity: Cu^{2+}

Design, synthesis, and biological evaluation of rutacecarpine derivatives as multitarget-directed ligands for the treatment of Alzheimer's disease

Mingfei Wu [a], Jie Ma [b], Lijun Ji [a], Min Wang [a], Jianfei Han [a], Zeng Li [a, *]

[a] *School of Pharmacy, Anhui Medical University, Hefei 230032, China*
[b] *The Central Hospital of Wuhan, Tongji Medical College of HUST, Wuhan 430000, China*

[*] Corresponding author. E-mail addresses: lizeng@ahmu.edu.cn (Z. Li).

Abstract

A series of 3-amino-substituted rutacecarpine derivatives were synthesized to identify novel multitarget-directed ligands (MTDLs) for the treatment of Alzheimer's disease (AD). Biological evaluation showed that most of the synthesized compounds inhibited butyrylcholinesterase (BuChE) and exerted antioxidant effects. Among the synthesized compounds, **6n** was subjected to further biological evaluation. Lineweaver–Burk plotting and molecular modeling illustrated that **6n** bound simultaneously to the peripheral anionic site (PAS) and catalytic sites (CAS) of BuChE. Furthermore, **6n** modulated Aβ aggregation; chelated biometals; presented good absorption, distribution, metabolism, excretion, and toxicity properties; and showed remarkable neuroprotective activity. Previous research has shown that the optimized compound **6n** has considerable potential for development as an MTDL for the treatment of AD.

Keywords: Alzheimer's disease, Rutacecarpine, Multitarget-directed ligands, Cholinesterases, Docking study, Drug-likeness prediction

1. Introduction

Alzheimer's disease (AD) is the most common cause of dementia among the elderly, and its main clinical manifestations are progressive memory loss and severe cognitive decline [1]. Its exact pathogenic mechanism remains unclear. Current research suggests that different factors are involved in the development of AD. The main pathological features of this disease include cholinergic neurotransmitter dysfunction in the hippocampal and cortical regions of the brain and the abnormal deposition of β-amyloid protein (Aβ), as well as oxidative stress, biometallic dysregulation, and neuroinflammation [2-4].

The reduction in the amount of cholinergic neurotransmitters is crucial for the pathogenesis of AD [5]. Acetylcholinesterase (AChE) and butyrylcholinesterase (BuChE) are two important types of cholinesterases (ChEs) in the central nervous system that can rapidly hydrolyze acetylcholine [6]. Under normal physiological conditions, AChE activity precedes BuChE activity. However, as AD progresses, the hydrolytic activity of AChE gradually decreases, whereas the activity of BuChE drastically increases [7]. ChE inhibitors, including tacrine, donepezil, galantamine, and rivastigmine, have been developed in recent years [8]. These inhibitors, however, induce numerous side effects, such as hepatotoxicity and digestive tract reactions, that severely affect therapeutic goals [9, 10]. Therefore, the development of effective and selective BuChE inhibitors may be an important approach for AD treatment and for avoiding the adverse reactions caused by AChE inhibitors during treatment [11, 12].

Neurofibrillary lesions composed of amyloid plaques formed through excessive Aβ production and deposition are a primary cause of AD [13]. Numerous plaques that are produced via Aβ aggregation are deposited in the hippocampal and basal ganglia regions of the brains of patients with AD [14]. Aβ oligomers are neurotoxic and can continuously activate inflammatory factors, such as IL-6 and NFTα [15]. Moreover, Aβ itself can act as an oxygen free radical donor that produces reactive oxygen

species (ROS) that directly affect the normal physiological functions of neurocytes [16, 17]. Furthermore, the biophysical disorders of biometallic ions, such as Cu^{2+}, Fe^{2+} and Zn^{2+}, are closely related to the pathogenesis of AD [18]. Metal ions, especially Cu^{2+}, have a strong affinity for Aβ and catalyze ROS production by participating in plaque formation [19]. Excessive ROS accumulation can result in oxidative stress and neuronal damage.

A growing body of evidence shows that the etiology of AD is extremely complex and involve different pathogenic factors that are correlated each other [20]. Therefore, the development of multitarget-directed ligands (MTDLs) that target multiple neuropathological processes has become a new approach for the treatment of AD [21]. Natural components have the advantages of low toxicity, limited side effects, and extensive pharmacological functions. Rutaecarpine (**Ru**, **Figure 1A**) is an important ingredient in the Chinese traditional medicine rutaceous evodia, which belongs to the pentacyclic indolopyridoquinazolinone alkaloid family [22]. **Ru** has multiple pharmacological activities, including antitumor, antioxidant, neuroprotection, and anti-inflammatory activities [23, 24]. The pharmacophore feature of **Ru** is similar to that of tacrine (9-amino-1, 2, 3, 4-tetrahydroacridine, THA, **Figure 1A**), which was first approved for use as an AChE inhibitor in 1993 [25]. Moreover, a series of novel **Ru** derivatives and related alkaloid derivatives, including 3-aminoalkanamide-substituted **Ru**, have been synthesized and shown to exert strong inhibitory activity when applied as selective AChE inhibitors [26-28].

A series of novel sulfonamide-based compounds with reversible and selective BuChE inhibitory effects [29, 30] at low nanomolar concentrations (IC_{50} = 4.91 nM) (**Figure 1B**) have been reported. Although **Ru** and sulfonamide groups exhibit ChE inhibitory activities, their combinations have not been applied as anti-AD agents. Thus, we designed and synthesized sulfonylamide-substituted **Ru** derivatives, a series of selective BuChE inhibitors, by hybridizing the pharmacophores of **Ru** with the sulfonamide group into one molecule (**Figure 1C**).

We aimed to establish **Ru**-based compounds on the basis of our preliminary work and literature review [26-28]. We focused on the synthesis of **Ru** derivatives with

anti-AD activities, including antioxidant, Aβ aggregation inhibition, and neuroprotective effects, as well as metal-chelating properties [31, 32]. We performed enzyme studies, molecular modeling , and drug-likeness evaluation to characterize the derivatives. Moreover, we summarized the structure–activity relationship of the derivatives to provide basic information for the development of anti-AD MTDLs based on the parental structure of **Ru**.

2. Results and discussion

2.1. Chemistry

The intermediate 3-amino-substituted **Ru** was prepared in accordance with the modified Bergman synthetic procedure [33]. A series of benzenesulfonyl chloride and thiazolesulfonyl chloride fragments replaced H in the 3-amino-substituted **Ru** to form an acylamino group. This reaction yielded the target benzenesulfonylamino-substituted or thiazolesulfonamide-substituted **Ru** derivatives.

As described in **Scheme 1**, isatoic anhydride was nitrated in concentrated H_2SO_4 in the presence of KNO_3 following the method reported by Iqbal [34]. Then, as shown in **Schemes 2**, a solution of nitroisoleic anhydride **1** in anhydrous pyridine was reacted through the one-pot method to obtain compound **2** in accordance with the Bergman method. The cyclization of compound **2** under acidic conditions afforded compound **3**. Compound **3** was dissolved in isopropanol and reduced with 80% hydrazine hydrate and 10% Pd/C to provide compound **4**. The CF_3H group of compound **4** was eliminated to obtain intermediate **5** with alcoholic KOH. Finally, intermediate **5** with a series of benzenesulfonyl chloride or thiazolesulfonyl chloride fragments was refluxed in anhydrous pyridine to induce an amide substitution reaction and acquire the desired derivatives **6a–p, 7a–c, and 8a**.

2.2. In vitro ChE inhibition and structure–activity relationships

The anti-ChE activity of the synthetic derivatives **6a–6p**, **7a–7c**, **8a** and the parental structure **Ru** were evaluated by using the method described by Ellman et al. [35] with tacrine and donepezil as reference drugs. The inhibitory activities of the compounds against AChE and BuChE are summarized in **Table 1**. Structure–activity relationships were explored, and active compounds with the highest activity were identified.

The experimental results revealed that all of the synthetic derivatives presented better inhibitory activity and selective effect on BuChE than the original parental structure (**Ru**). The compounds presented a weak or nonexistent inhibitory effect on AChE. Compounds **6m**, **6n**, and **6o** showed the best inhibitory activity against BuChE with the IC_{50} values of 3.82 ± 0.68, 3.60 ± 0.34, and 3.95 ± 0.72 μM, respectively. These results prove that the introduction of the aromatic sulfonamide-substituted group could drastically strengthen the inhibitory activity of the derivatives. The inhibitory activities of the reference drugs tacrine and donepezil against AChE and BuChE were quantified under the same assay conditions. Tacrine and donepezil provided IC_{50} values of 0.28 ± 0.026 and 0.04 ± 0.007 μM for AChE, respectively, and 0.02 ± 0.01 and 7.87 ± 1.24 μM for BuChE, respectively.

Structure–activity relationship analysis showed that the derivatives with sulfonamide groups connected to different aromatic nuclei expressed different degrees of ChE inhibitory activity. The inhibitory activity of derivatives with benzene rings was strong and was 20-fold higher than that of derivatives with thiophene rings. For example, the inhibitory activity of compounds **6a–6p** (IC_{50}: 3.60 ± 0.34–25.78 ± 1.31 μM) against BuChE was significantly stronger than that of compounds **7a–7c** and **8a** ($IC_{50} \geq 60.34 \pm 4.03$ μM). Moreover, the electronegativity of the substituent base on the aromatic ring had a significant effect on the inhibitory activity of the compounds, and the compounds with strong electron withdrawing group on the benzene ring had significant inhibitory activity for BuChE, such as compounds **6i, 6k**, **6l**, **6m**, **6n** and **6o**. In addition, with the volume increase of the substituent of aromatic ring, the inhibitory activity for BuChE enhanced observably. The inhibitory activities of derivatives against BuChE gradually increased (IC_{50} value: **6k** = 7.57 ± 0.77 μM, **6l** = 8.28 ± 0.91 μM, **6o** = 3.95 ± 0.72 μM) when −F, $-CF_3$, or $-OCF_3$ was introduced into

the C4 positions of their benzene rings. Moreover, the introduction of substituents at the C2, C3, and C4 positions of benzene rings resulted in inhibitory activities with different intensities. The effectiveness of the derivative with a $-CF_3$ in the C3 position was 2-fold that of the derivative with a $-CF_3$ in the C4 position (IC_{50} value: **6m** = 3.82 ± 0.68 μM, **6l** = 8.28 ± 0.91 μM). This trend was also demonstrated by other compounds. The effectiveness of the derivative with a $-OCF_3$ substituent in the C2 position was better than that of the derivative with a $-OCF_3$ substituent in the C4 position (IC_{50} value: **6n** = 3.60 ± 0.34 μM, **6o** = 3.95 ± 0.72 μM).

2.3. Kinetic study of BuChE inhibition

Compound **6n**, the derivative with the highest inhibitory activity, was subjected to enzyme kinetics analysis to determine the kinetics of BuChE inhibition. The slopes and intercepts of the reciprocal Lineweaver–Burk plot presented in **Figure 2** increased with the increase in inhibitor concentration. The intersection of each trend line in the fourth quadrant indicated a mixed-type inhibitory mode. This result suggests that compound **6n** bound to BuChE at the catalytic active site (CAS) and peripheral anionic (PAS) site.

2.4. Docking analysis of compounds through enzyme and molecular dynamics simulation

Molecular modeling can be used to determine interactions between ligands and receptors [36, 37]. The most stable conformation in the active site was illustrated and analyzed through 2D and 3D diagrams and on the basis of the -*CDOCKER-INTERACTION-ENERGY* scores generated by the *CDOCKER* program, which was verified as docking protocol by re-docking of the co-crystallized ligand 92H into 5NN0 active site. The docking pose of 92H was compared with the initial pose using root mean square deviation (RMSD) and 92H docked almost at the same position (RMSD = 0.3193 Å, see supporting information for details, **Table S1**). The highest score provided by -*CDOCKER_INTERACTION_ENERGY* for compound **6n**

within BuChE was 45.9637 kcal/mol. The H bond surface of the BuChE receptor with compound **6n** indicates that compound **6n** has strong affinity for BuChE **(Figure 3A)**. The 2D diagram shows that one conventional H bond interaction was generated by connecting the F atom of trifluoromethoxy group at the C2 position of the aromatic ring with the OH group of THR120 (distance = 2.12 Å). Three C–H bond interactions were also produced between the F atoms of the trifluoromethoxy group with the CH_2 group of GLY116 (distance = 2.82 Å), GLY121 (distance = 2.82 Å) and THR120 (distance = 3.00 Å). Moreover, three halogen interactions occurred between F atoms of the trifluoromethoxy group with the C=O group of THR82 (distance = 3.00 and 2.98 Å) and GLY115 (distance = 2.91 Å). One π–sulfur interaction occurred in sulfonamide with TRP82 (distance = 4.24 Å). One π–π t–shaped interaction generated in benzene ring with TRP82 (distance = 4.15 Å). The above results confirm that the introduction of the side-chain substituent of the sulfonamide aromatic group drastically improved the binding between compound **6n** and BuChE. Furthermore, the quinazolinocarboline core structure of compound **6n** created a C–H bond interaction with SER287 (distance = 2.82 Å) and three hydrophobic interactions, which included one π–sigma interactions with PRO285 (distance = 2.61 Å) and two π–π stacked interactions with TYP332 (distance = 5.91 and 5.64 Å) (**(Figure 3B)**.

Molecular dynamics (MD) simulation was performed to verify the structural constancy of the system **6n**-BuChE [38]. The convergence and stability of the system were monitored by evaluating the RMSD values of the backbone atoms with respect to the initial conformation [39]. The system **6n**-BuChE were subjected to the 10000 ps MD simulations. **Figure 4** shows that after 7000 ps, the wave range of RMSD was within 1 Å, which corresponds to a near-identical degree of postural similarity. The MD simulation results suggest that compound **6n** and BuChE formed a stable combination and were consistent with the results of molecular docking.

2.5. DPPH radical scavenging activity

1,1-Diphenyl-2-picrylhydrazyl (DPPH) is an extremely effective free radical

scavenger that can be used to monitor a chemical reaction that involves free radicals [40, 41]. The DPPH assay was performed with ascorbic acid and donepezil as reference antioxidants to evaluate the ability of the synthesized compounds to scavenge activated oxygen species. As shown in **Table 1**, all of the synthesized compounds exhibited mild free radical scavenging activity with the DPPH RP of 35.18%–59.32% at a concentration of 100 μM.

2.6. Determination of intracellular ROS production

The extensive accumulation of endogenous ROS can accelerate the progression of AD by causing oxidative stress and triggering nerve damage [42]. The antioxidant potency of compound **6n** against intracellular ROS generation was investigated in H_2O_2-treated SH-SY5Y and PC12 cells through the 2',7'-dichlorodihydrofluorescein diacetate (DCFH-DA) assay [43]. Cells were treated with compound **6n** at concentrations of 1, 5, 10, 20, and 50 μM and then exposed to H_2O_2 (250 μM) for 18 h. Intracellular ROS content was measured by using the DCFH-DA probe (10 μM). As shown in **Figure 5A and 5B**, the amount of intracellular ROS generation in control group increased significantly relative to that in blank group with the percentage of 119.61% in SH-SY5Y cells model and 136.41% in PC12 cells model, respectively. ROS levels in **6n** treated group almost reduced to the blank group level in a concentration-independent manner (see supporting information for details, **Table S2**). Therefore, compound **6n** can effectively reduce H_2O_2-induced intracellular ROS accumulation. This result provides further evidence that compound **6n** is a promising neuroantioxidant.

2.7. Effect on Aβ peptide aggregation

The self-assembly of Aβ peptide into fibers promotes the formation of senile plaques and ROS by inducing aggregation effects and participating in redox reactions in the body [44]. Therefore, the ability of the representative compound **6n** to inhibit self-mediated Aβ aggregation was assessed through the thioflavin T (ThT)

fluorometry method [45]. As shown in **Table 2**, the inhibitory potency of **Ru** (11.25%) against Aβ (1-42) peptide self-aggregation was lower than that of the reference drug donepezil (33.78%). The **Ru** derivative **6n** prevented self-mediated Aβ aggregation with an inhibition rate of 58.95%. The inhibition rate of **6n** was superior to that of **Ru** and the reference drug donepezil. Therefore, the structural modification of the parental structure **Ru** significantly improved biological activity.

Transmission electron microscopy (TEM) was employed to explore whether the morphology of Aβ aggregates had changed [46, 47]. Aβ (1-42) samples incubated for 0 h alone did not aggregate and appeared dispersed **(Figure 6A)**. However, after 48 h of incubation, the majority of Aβ (1-42) self-aggregated into amyloid fibers, and numerous mature and bulky fibers were observed (**Figure 6B**). Aggregation in Aβ (1-42) samples incubated with compound **6n** and donepezil decreased. Compound **6n** inhibited Aβ aggregation more effectively than donepezil (**Figures 6C** and **6D**) as indicated by the thin and short fibers observed in Aβ (1-42) samples incubated with compound **6n**. TEM results further demonstrate that compound **6n** could inhibit Aβ aggregation and are consistent with the ThT assay results.

2.8. Metal-chelating property

The chelation of antioxidants with biometal ions has become a strategy for the treatment of AD because it can prevent amyloid plaque formation and reduce oxidative stress levels [48, 49]. The chelation activity of compound **6n** against biometal ions, such as Cu^{2+}, Fe^{2+}, Zn^{2+}, Al^{3+}, Mg^{2+} and Ca^{2+}, in amyloid plaques was investigated through UV–vis spectrometry.

Figure 7A shows that the UV spectra of the methanolic solution of compound **6n** changed after the addition of $CuCl_2$ solution relative to those of the methanolic solutions of compound **6n** after the addition of $FeSO_4$, $ZnCl_2$, $AlCl_3$, $MgCl_2$, and $CaCl_2$. The reduction in maximum absorption intensity at 352 and the appearance of a shoulder at 370 nm upon the addition of $CuCl_2$ solution to the compound **6n** solution indicated that complexes had formed. The chelating properties of compound **6n** could

be attributed to the presence of the carbonyl and sulfonamide groups in the compound.

The stoichiometry of the Cu^{2+}−**6n** complex was also determined through the molar ratio method by using $CuCl_2$ solutions with increasing concentrations to titrate a methanolic solution of compound **6n** (20 μM). **Figure 7B** shows that absorbance gradually increased at 382 nm and then stabilized. The intersection of two straight lines at the mole fraction of 1.1 indicates a stoichiometric ratio of Cu^{2+}/**6n** complex of 1:1.

2.9. Oil/water partition coefficient assay and ADMET prediction of active compounds

The physicochemical parameters of a drug are correlated with the membrane permeability of the body. Lipinski's rule of five is used as the rule of thumb when assessing whether a compound can be used as an oral drug [50, 51]. For example, the oil/water partition coefficient, which is expressed as a log P value, can reflect the absorption of a drug in an organism [52]. The oil/water partition coefficients of compounds that showed strong potency in bioactivity assessment were measured. **Table 3** shows that the log P values of compounds **6k**, **6l**, **6h**, **6m**, **6n**, **6i**, **6o**, and **7b** ranged from 2.25 to 3.62. These results imply that the active compounds were lipophilic (log P < 5).

The absorption, distribution, metabolism, excretion, and toxicity (ADMET) properties of the selected eight compounds were also predicted by using DS 2017 R2 [53]. The different descriptors of ADMET characteristics have different prediction levels. Compounds with low prediction levels have good ADMET properties. **Table 4 and Figure 8** show that these compounds likely demonstrate good absorption in the human intestine (HIA levels of 0), good solubility in water at 25 °C (solubility levels of 1 and 2) and moderate blood–brain barrier permeability. Moreover, the results show that these compounds are noninhibitors of CYP2D6 (CYP2D6 level of 0) and are highly likely to bind to plasma proteins. In addition, the data revealed that the selected compounds met the PSA2D and ALogP98 requirements within the 95% and 99%

confidence limit ellipses of the BBB permeation and HIA models, respectively.

2.10. Neuroprotection study

Neurotoxicity caused by H_2O_2-induced oxidative damage considerably accelerates the progression of neurodegenerative diseases [54]. Therefore, the potential protective effects of the synthetic derivatives **6a–6p, 7a–7c,** and **8a** against H_2O_2-induced oxidative stress were evaluated by using PC12 cells. PC12 cells were pretreated for 4 h with different concentrations (1, 5, 10, 30, and 50 μM) of the compounds prior to treatment with H_2O_2 (250 μM). Cell viability was measured after 24 h of treatment by using the MTT assay. As seen in **Table 5,** the survival rate of PC12 cells incubated without the derivatives fell in the range of 35.69%–50.26%. The viability of PC12 cells incubated with various concentrations of compounds, especially compounds **6h**, **6i**, **6l**, **6o**, **6n**, **6p**, and **7b**, increased in a concentration-dependent manner. The neuroprotective effect of compounds **6h**, **6o** and **6n** were higher than that of reference drug quercetin. The protective effects of compounds **6a**, **6b**, **6c**, **6f**, **6g**, **6j**, **6k**, **6m**, **7a**, and **7c** were weaker than that of the control treatment. Compounds **6d**, **6e**, and **8a** did not show a significant protective effect against H_2O_2-induced cytotoxicity at all concentrations.

The human neuroblastoma SH-SY5Y cell line was also used to assess H_2O_2-induced cytotoxicity and Aβ, which contribute to neuronal cell death, to validate the neuroprotective potency of compound **6n**. **Figure 9** shows that the viability of SH-SY5Y cells treated with compound **6n** (10, 30, and 50 μM) significantly increased relative to that of cells treated with the control. Survival rate increased in a dose-dependent manner. Moreover, comparing the H_2O_2 **(Figure 9A)** and Aβ **(Figure 9B)** groups revealed that the cell viability of the H_2O_2 group (60.58%) was higher than that of the Aβ group (57.84%) with compound **6n** at 30 μM (see supporting information for details, **Table S3**).

3. Conclusions

A series of novel 3-sulfonamide-substituted **Ru** derivatives were designed, synthesized, and biologically evaluated for use as novel MTDLs for the development of potential anti-AD agents. The results of biological evaluation showed that most of the synthesized compounds presented selective inhibitory activity against BuChE. Compound **6n** was identified as the most potent BuChE inhibitor with IC_{50} = 3.60 ± 0.34 μM. The results of enzyme kinetics analysis suggest that compound **6n** inhibited BuChE through a mixed-type mode by binding to the CAS and PAS. Molecular modeling and MD simulation results showed that compound **6n** could bind strongly to BuChE. Moreover, compound **6n** could effectively reduce H_2O_2-induced intracellular ROS accumulation. This result demonstrates that compound **6n** could act as a novel antioxidant. Furthermore, compound **6n** may potentially prevent the production of amyloid plaques by strongly inhibiting self-induced Aβ aggregation with a percentage of inhibition of 58.95%. This result was also confirmed through TEM. Compound **6n** could selectively chelate with biometal ion Cu^{2+} and showed good drug-likeness and ADMET properties as indicated by its physicochemical parameters. It also demonstrated remarkable neuroprotective effects against H_2O_2- and Aβ-induced neurotoxicity toward PC12 and SH-SY5Y cell lines. The above results strongly suggest that compound **6n** is a promising MTDL. The further structural optimization of 3-sulfonamide-substituted **Ru** derivatives as potential lead candidates is encouraged for the development of new anti-AD drugs.

4. Experimental section

4.1. Chemistry

All common chemicals were obtained from commercial sources and used without further purification. Reaction progress was monitored using analytical thinlayer chromatography (TLC) on precoated silica gel HSGF254 plates(Qingdao Haiyang Chemical Plant, China). Column chromatography was performed on silica gel (200-300 mm; Qingdao Dingkang Chemical Inc.). ^{1}H NMR and ^{13}C NMR spectra were measured using TMS (δ 0 ppm) as the internal standard in dimethyl sulfoxide

(DMSO-d6) solutions with a Bruker 400 MHz instrument (Bruker, Germany). The MS spectra was recorded on Q Exactive™ Plus mass spectrometry (Thermofisher, USA).

4.1.1. Intermediate 3-amino-substituted rutaecarpine (**5**)

To a solution of isatoic anhydride (20 g, 122.7 mmol) in con. H_2SO_4 (30 mL) at 0 °C was added Potassium nitrate (12.40 g, 122.7 mmol). The reaction was stirred for 1 h. The mixture was poured into cold water, and the precipitate formed was collected and dried to afford nitro compound **1**. Compound **1** dissolving (5.2 g) in the anhydrous pyridine (100 mL) was dropwise add with the mixture solution of trifluoroacetic anhydride (3.7 mL) and anhydrous pyridine (4 mL) at room temperature. The stirring was refluxed for 30 min. Then, tryptamine (4.0 g) was added and refluxed for additional 1 h. The reaction solution was cooled and poured into ice water. The precipitate was filtrated and dried to give compound **2**. A solution of compound **2** (8.0 g) in acetic acid (40 mL) and of hydrochloric acid (6 mL) was refluxed for 1 h. After cooling, ice water was add to precipitate compound **3.** compound **3 (**4.0 g**)** was hydrogenated by 10% Pd/C (1.2 g) and 80% hydrazine hydrate (10mL) in isopropanol at 80□ for 1h. After the reaction was completed, Pd/C was filtered off. The hydrazine hydrate was evaporated to remove to obtain compound **4**. Compound **4 (**3.7 g) with KOH (4.0 g) were added to a solution of water (15 mL) and ethanol (50 mL), and the mixture was refluxed for 1 h. After cooling the reaction mixture, a large amount of yellow-brown precipitate was formed, and the precipitate was filtered and recrystallizated by hot methanol to give intermediate 3-amino-substituted rutaecarpine **5** as pale yellow powder, in a yield of 35%. ^{1}H NMR (400 MHz, DMSO) δ 11.73 (s, 1H), 7.61 (d, *J* = 7.9 Hz, 1H), 7.45 (dd, *J* = 8.3, 3.7 Hz, 2H), 7.28 (s, 1H), 7.22 (t, *J* = 7.3 Hz, 1H), 7.08 (dd, *J* = 16.5, 8.7 Hz, 2H), 5.69 (s, 2H), 4.42 (t, *J* = 6.7 Hz, 2H), 3.13 (t, *J* = 6.7 Hz, 2H). ^{13}C NMR (101 MHz, DMSO) δ 160.94, 148.11, 141.35, 138.75, 138.57, 128.20, 128.01, 125.60, 124.45, 122.86, 122.32, 119.99, 119.99, 116.18, 112.80, 107.67, 41.24, 19.52. HRMS (ESI)

m/z $[M + H]^+$: 303.1238 calcd for $C_{24}H_{17}BrN_4O_3S$: 303.1235;

4.1.2. General procedure for the preparation of desired derivatives **6a-6p, 7a-7c, and 8a**.

A solution of the appropriate acid halide fragments (4.8 mmol) in dry pyridine (5 mL) was dropwise added to a well-stirred mixture of the intermediate 3-amino-substituted rutaecarpine **5** (4 mmol) in dry pyridine (50 mL) at room temperature. The reaction was stirred for 30 min and monitored by TLC. After the reaction completed, the pH was adjusted to neutral with dilute hydrochloric acid. The pyridine and residual sulfonyl chloride were distilled under reduced pressure. The mixture was extracted with an ethyl acetate-water system. The aqueous layer was discarded and ethyl acetate was evaporated to obtain crude product. The crude product was washed with water and dried under vacuum. The solid residue was purified by flash chromatography on silica gel with ethyl acetate/petroleum ether (1:1) elution to provide the desired derivatives **6a-6p, 7a-7c, and 8a**.

4.1.2.1. 3-(4-methoxybenzenesulfonamide)-rutaecarpine (**6a**)

The intermediate **5** was treated with 4-methoxybenzenesulfonyl chloride according to the general procedure mentioned above to get compound **6a** as white powder, in a yield of 65%; ^{1}H NMR (400 MHz, DMSO-D6) δ 11.80 (s, 1H), 10.50 (s, 1H), 7.85 – 7.77 (m, 1H), 7.68 (d, *J* = 8.8 Hz, 2H), 7.59 (d, *J* = 7.9 Hz, 1H), 7.55 (d, *J* = 8.8 Hz, 1H), 7.53 – 7.49 (m, 1H), 7.41 (d, *J* = 8.5 Hz, 1H), 7.21 (t, *J* = 7.7 Hz, 1H), 7.04 (t, *J* = 7.6 Hz, 3H), 4.36 (t, *J* = 6.8 Hz, 2H), 3.73 (s, 3H), 3.10 (t, *J* = 6.8 Hz, 2H). ^{13}C NMR (101 MHz, DMSO) δ 163.02, 160.67, 144.85, 144.30, 139.06, 136.25, 131.25, 129.37, 128.19, 127.54, 127.46, 125.36, 125.11, 121.60, 120.33, 120.17, 117.99, 116.39, 114.97, 112.96, 56.09, 56.09, 41.37, 19.35, 19.11. HRMS (ESI) m/z $[M + H]^+$: 473.1273 calcd for $C_{24}H_{17}BrN_4O_3S$: 473.1275;

4.1.2.2. 3-(2,4-dimethoxybenzenesulfonamide)-rutaecarpine (**6b**)

The intermediate **5** was treated with 2,4-dimethoxybenzenesulfonyl chloride according to the general procedure mentioned above to get compound **6b** as brown powder, in a yield of 63%; ^{1}H NMR (400 MHz, DMSO) δ 11.82 (s, 1H), 10.31 (s, 1H), 7.85 (s, 1H), 7.73 (d, *J* = 8.8 Hz, 1H), 7.63 (d, *J* = 8.0 Hz, 1H), 7.56 (s, 2H), 7.45 (d, *J* = 8.2 Hz, 1H), 7.25 (d, *J* = 7.5 Hz, 1H), 7.08 (t, *J* = 7.5 Hz, 1H), 6.71 – 6.50 (m, 2H), 4.39 (t, *J* = 6.8 Hz, 2H), 4.03 (q, *J* = 7.0 Hz, 1H), 3.88 (s, 3H), 3.77 (s, 3H), 3.14 (t, *J* = 6.8 Hz, 2H), 1.99 (s, 1H), 1.19 (dd, *J* = 18.3, 11.2 Hz, 2H). ^{13}C NMR (101 MHz, DMSO) δ 165.13, 160.67, 158.44, 144.61, 143.88, 139.02, 136.57, 132.58, 127.90, 127.58, 126.83, 125.21, 121.51, 120.23, 118.67, 117.85, 115.55, 112.94, 105.54, 99.66, 60.24, 56.72, 56.19, 41.34, 19.35, 14.54. HRMS (ESI) m/z $[M + H]^+$: 503.1374 calcd for $C_{24}H_{17}BrN_4O_3S$: 503.1276;

4.1.2.3. 3-(3,4-dimethoxybenzenesulfonamide)-rutaecarpine (**6c**)

The intermediate **5** was treated with 3,4-dimethoxybenzenesulfonyl chloride according to the general procedure mentioned above to get compound **6c** as white powder, in a yield of 46%; ^{1}H NMR (400 MHz, DMSO-D6) δ 11.80 (s, 1H), 10.45 (s, 1H), 7.84 (s, 1H), 7.55 (ddd, *J* = 14.5, 11.1, 5.0 Hz, 3H), 7.41 (d, *J* = 8.3 Hz, 1H), 7.30 (d, *J* = 10.5 Hz, 2H), 7.21 (t, *J* = 7.6 Hz, 1H), 7.04 (t, *J* = 8.7 Hz, 2H), 4.36 (t, *J* = 6.0 Hz, 2H), 3.31 (d, *J* = 2.3 Hz, 9H), 3.10 (t, *J* = 6.2 Hz, 2H). ^{13}C NMR (101 MHz, DMSO) δ 161.44, 160.62, 158.91, 145.16, 144.86, 139.09, 137.08, 135.27, 129.68, 128.69, 128.60, 128.40, 128.08, 127.47, 125.33, 125.16, 121.65, 121.51, 121.32, 120.34, 120.17, 118.84, 118.61, 118.16, 117.45, 112.98, 41.39, 19.33. HRMS (ESI) m/z $[M + H]^+$: 503.1378 calcd for $C_{24}H_{17}BrN_4O_3S$: 503.1377;

4.1.2.4. 3-(4-nitrobenzenesulfonamide)-rutaecarpine (**6d**)

The intermediate **5** was treated with 4-nitrobenzenesulfonyl chloride according to the general procedure mentioned above to get compound **6d** as yellow powder, in a yield of 52%; ^{1}H NMR (400 MHz, DMSO-D6) δ 11.81 (s, 1H), 10.94 (s, 1H), 8.34 (d, *J* = 8.8 Hz, 2H), 7.98 (d, *J* = 8.6 Hz, 2H), 7.83 (d, *J* = 2.2 Hz, 1H), 7.59 (dd, *J* = 8.4,

3.5 Hz, 2H), 7.53 (dd, *J* = 8.8, 2.2 Hz, 1H), 7.41 (d, *J* = 8.2 Hz, 1H), 7.21 (t, *J* = 7.6 Hz, 1H), 7.04 (t, *J* = 7.5 Hz, 1H), 4.36 (t, *J* = 6.8 Hz, 2H), 3.10 (t, *J* = 6.8 Hz, 2H). ^{13}C NMR (101 MHz, DMSO) δ 160.60, 150.39, 145.18, 145.03, 144.89, 139.09, 135.14, 128.74, 128.74, 128.44, 128.09, 127.45, 125.33, 125.25, 125.25, 125.20, 121.66, 120.38, 120.21, 118.20, 117.45, 112.98, 41.39, 19.33. HRMS (ESI) m/z $[M + H]^+$: 488.1013 calcd for $C_{24}H_{17}BrN_4O_3S$: 488.1012;

4.1.2.5. 3-(3-nitrobenzenesulfonamide)-rutaecarpine (**6e**)

The intermediate **5** was treated with 3-nitrobenzenesulfonyl chloride according to the general procedure mentioned above to get compound **6e** as pale brown powder, in a yield of 58%; ^{1}H NMR (400 MHz, DMSO-D6) δ 11.80 (s, 1H), 10.89 (s, 1H), 8.50 (s, 1H), 8.41 (dd, *J* = 8.2, 1.1 Hz, 1H), 8.11 (d, *J* = 7.9 Hz, 1H), 7.41 (d, *J* = 8.3 Hz, 1H), 7.20 (t, *J* = 7.6 Hz, 1H), 7.02 (t, *J* = 7.4 Hz, 1H), 4.35 (t, *J* = 6.8 Hz, 2H), 3.09 (t, *J* = 6.8 Hz, 2H). ^{13}C NMR (101 MHz, DMSO) δ 160.59, 148.37, 145.21, 144.97, 141.11, 139.09, 135.03, 133.05, 131.99, 128.45, 128.27, 128.21, 127.44, 125.31, 125.18, 121.89, 121.65, 120.35, 120.18, 118.19, 117.66, 112.97, 41.38, 19.32. HRMS (ESI) m/z $[M + H]^+$: 488.1013 calcd for $C_{24}H_{17}BrN_4O_3S$: 488.1011;

4.1.2.6. 3-(4-bromobenzenesulfonamide)-rutaecarpine (**6f**)

The intermediate **5** was treated with 4-bromobenzenesulfonyl chloride according to the general procedure mentioned above to get compound **6f** as white powder, in a yield of 59%; ^{1}H NMR (400 MHz, DMSO-D6) δ 11.80 (s, 1H), 10.50 (s, 1H), 7.85 – 7.77 (m, 1H), 7.68 (d, *J* = 8.8 Hz, 2H), 7.59 (d, *J* = 7.9 Hz, 1H), 7.55 (d, *J* = 8.8 Hz, 1H), 7.53 – 7.49 (m, 1H), 7.41 (d, *J* = 8.5 Hz, 1H), 7.21 (t, *J* = 7.7 Hz, 1H), 7.04 (t, *J* = 7.6 Hz, 3H), 4.36 (t, *J* = 6.8 Hz, 2H), 3.73 (s, 3H), 3.10 (t, *J* = 6.8 Hz, 2H). ^{13}C NMR (101 MHz, DMSO) δ 160.64, 145.06, 144.67, 139.08, 138.88, 135.59, 133.00, 133.00, 129.13, 129.13, 128.34, 127.86, 127.54, 127.49, 125.34, 125.16, 121.63, 120.36, 120.19, 118.12, 117.03, 112.98, 41.39, 19.34. HRMS (ESI) m/z $[M + H]^+$: 523.0252 calcd for $C_{24}H_{17}BrN_4O_3S$: 523.0253;

4.1.2.7. 3-(2,6-dichlorobenzenesulfonamide)-rutaecarpine **(6g)**

The intermediate **5** was treated with 2,6-dichlorobenzenesulfonyl chloride according to the general procedure mentioned above to get compound **6g** as white powder, in a yield of 65%; ^{1}H NMR (400 MHz, DMSO) δ 11.86 (s, 1H), 10.92 (s, 1H), 8.00 (s, 4H), 7.89 (s, 1H), 7.60 (dt, *J* = 8.9, 5.1 Hz, 3H), 7.47 (d, *J* = 8.2 Hz, 1H), 7.26 (t, *J* = 7.6 Hz, 1H), 7.08 (t, *J* = 7.4 Hz, 1H), 4.41 (s, 2H), 3.15 (t, *J* = 6.7 Hz, 2H). ^{13}C NMR (101 MHz, DMSO) δ 160.62, 145.14, 144.80, 143.55, 139.09, 135.31, 133.35, 133.03, 128.40, 128.14, 127.91, 127.47, 127.18, 127.18, 125.33, 125.15, 122.42, 121.66, 120.34, 120.17, 118.14, 117.17, 112.97, 41.38, 19.32. HRMS (ESI) m/z [M + H]$^{+}$: 511.1036 calcd for $C_{24}H_{17}BrN_4O_3S$: 511.1038;

4.1.2.8. 3-(3,5-dichlorobenzenesulfonamide)-rutaecarpine (**6h**)

The intermediate **5** was treated with 3,5-dichlorobenzenesulfonyl chloride according to the general procedure mentioned above to get compound **6h** as brown powder, in a yield of 52%; ^{1}H NMR (400 MHz, DMSO-D6) δ 11.81 (s, 1H), 10.81 (s, 1H), 7.93 (s, 1H), 7.81 (s, 1H), 7.71 (s, 2H), 7.63 – 7.50 (m, 3H), 7.42 (d, *J* = 8.2 Hz, 1H), 7.21 (t, *J* = 7.5 Hz, 1H), 7.03 (t, *J* = 7.3 Hz, 1H), 4.36 (t, *J* = 6.7 Hz, 2H), 3.10 (t, *J* = 6.7 Hz, 2H). ^{13}C NMR (101 MHz, DMSO) δ 160.61, 145.27, 145.01, 142.68, 139.11, 135.69, 135.69, 134.96, 133.36, 128.48, 128.19, 127.47, 125.67, 125.67, 125.33, 125.18, 121.67, 120.37, 120.18, 118.22, 117.67, 112.99, 41.40, 19.33. HRMS (ESI) m/z [M + H]$^{+}$: 511.0384 calcd for $C_{24}H_{17}BrN_4O_3S$: 511.0389;

4.1.2.9. 3-(3-chloro-4-fluorobenzenesulfonamide)-rutaecarpine (**6i**)

The intermediate **5** was treated with 3-chloro-4-fluorobenzenesulfonyl chloride according to the general procedure mentioned above to get compound **6i** as white powder, in a yield of 48%; ^{1}H NMR (400 MHz, DMSO-D6) δ 11.81 (s, 1H), 10.73 (s, 1H), 7.94 (d, *J* = 6.6 Hz, 1H), 7.81 (s, 1H), 7.75 – 7.68 (m, 1H), 7.64 – 7.50 (m, 4H), 7.42 (d, *J* = 8.2 Hz, 1H), 7.21 (t, *J* = 7.6 Hz, 1H), 7.03 (t, *J* = 7.5 Hz, 1H), 4.36 (t, *J* =

6.5 Hz, 2H), 3.10 (t, *J* = 6.5 Hz, 2H). ^{13}C NMR (101 MHz, DMSO) δ 160.69, 152.73, 149.02, 144.86, 144.33, 139.05, 136.26, 131.00, 128.16, 127.59, 127.53, 125.35, 125.12, 121.54, 121.10, 120.33, 120.18, 118.01, 116.53, 112.96, 111.60, 109.81, 56.22, 56.17, 41.37, 19.33. HRMS (ESI) m/z $[M + H]^+$: 495.0682 calcd for $C_{24}H_{17}BrN_4O_3S$: 495.0680;

4.1.2.10. 3-(4-tert-butylbenzenesulfonamide)-rutaecarpine (**6j**)

The intermediate **5** was treated with 4-tert-butylbenzenesulfonyl chloride according to the general procedure mentioned above to get compound **6j** as white powder, in a yield of 53%; ^{1}H NMR (400 MHz, DMSO-D6) δ 11.80 (s, 1H), 10.64 (s, 1H), 7.86 (s, 1H), 7.69 (d, *J* = 8.4 Hz, 2H), 7.62 – 7.53 (m, 4H), 7.41 (d, *J* = 8.3 Hz, 1H), 7.21 (t, *J* = 7.5 Hz, 1H), 7.05 (d, *J* = 7.5 Hz, 1H), 4.36 (t, *J* = 6.8 Hz, 2H), 3.50 (s, 1H), 3.10 (t, *J* = 6.8 Hz, 2H), 1.20 (s, 10H). ^{13}C NMR (101 MHz, DMSO) δ 160.67, 156.58, 144.86, 144.24, 139.06, 137.08, 136.19, 128.27, 127.52, 127.17, 126.99, 126.99, 126.77, 126.77,125.36, 125.14, 121.64, 120.36, 120.19, 118.01, 116.00, 112.97, 41.39, 35.35, 31.15, 31.15, 31.15, 19.36. HRMS (ESI) m/z $[M + H]^+$: 499.1787 calcd for $C_{24}H_{17}BrN_4O_3S$: 499.1786;

4.1.2.11. 3-(4-fluorobenzenesulfonamide)-rutaecarpine (**6k**)

The intermediate **5** was treated with 4-fluorobenzenesulfonyl chloride according to the general procedure mentioned above to get compound **6k** as white powder, in a yield of 61%; ^{1}H NMR (400 MHz, DMSO-D6) δ 11.80 (s, 1H), 10.65 (s, 1H), 7.80 (dd, *J* = 8.4, 3.9 Hz, 3H), 7.61 – 7.48 (m, 3H), 7.44 – 7.34 (m, 3H), 7.21 (t, *J* = 7.6 Hz, 1H), 7.04 (t, *J* = 7.4 Hz, 1H), 4.36 (t, *J* = 6.8 Hz, 2H), 3.10 (t, *J* = 6.8 Hz, 2H). ^{13}C NMR (101 MHz, DMSO) δ 166.13, 163.62, 160.64, 145.03, 144.61, 139.08, 136.00, 135.73, 130.27, 130.18, 128.29, 127.87, 127.49, 125.34, 125.15, 121.61, 120.34, 120.18, 118.09, 117.22, 117.00, 112.97, 41.38, 19.33. HRMS (ESI) m/z $[M + H]^+$: 461.1069 calcd for $C_{24}H_{17}BrN_4O_3S$: 461.1068;

494 4.1.2.12. 3-[4-(trifluoromethyl)benzenesulfonamide]-rutaecarpine (**6l**)

495 The intermediate **5** was treated with 4-(trifluoromethyl)benzenesulfonyl chloride
496 according to the general procedure mentioned above to get compound **6l** as pale
497 brown powder, in a yield of 47%; ^{1}H NMR (400 MHz, DMSO-D6) δ 11.81 (s, 1H),
498 10.87 (s, 1H), 7.94 (s, 1H), 7.82 (d, *J* = 2.2 Hz, 1H), 7.56 (ddd, *J* = 10.8, 8.4, 3.6 Hz,
499 1H), 7.41 (d, *J* = 8.3 Hz, 1H), 7.21 (t, *J* = 7.6 Hz, 1H), 7.04 (t, *J* = 7.5 Hz, 1H), 4.36 (s,
500 1H), 3.11 (t, *J* = 6.7 Hz, 1H). ^{13}C NMR (101 MHz, DMSO) δ 160.66, 151.61, 145.00,
501 144.57, 139.09, 138.75, 135.88, 129.77, 129.77, 128.33, 127.92, 127.51, 125.35,
502 125.14, 121.98, 121.98, 121.65, 120.35, 120.18, 118.09, 116.99, 112.98, 41.38, 19.34.
503 HRMS (ESI) m/z $[M + H]^+$: 511.1042 calcd for $C_{24}H_{17}BrN_4O_3S$: 511.1041;

504 4.1.2.13. 3-[3-(trifluoromethyl)benzenesulfonamide]-rutaecarpine (**6m**)

505 The intermediate **5** was treated with 3-(trifluoromethyl)benzenesulfonyl chloride
506 according to the general procedure mentioned above to get compound **6m** as pale
507 brown powder, in a yield of 52%; ^{1}H NMR (400 MHz, DMSO-D6) δ 11.81 (s, 1H),
508 10.77 (s, 1H), 8.00 (dd, *J* = 12.5, 6.7 Hz, 3H), 7.78 (dd, *J* = 10.8, 5.0 Hz, 2H), 7.59
509 (dd, *J* = 8.5, 3.2 Hz, 2H), 7.52 (dd, *J* = 8.8, 2.5 Hz, 1H), 7.41 (d, *J* = 8.3 Hz, 1H), 7.21
510 (ddd, *J* = 8.2, 7.0, 1.1 Hz, 1H), 7.04 (ddd, *J* = 8.0, 7.1, 0.9 Hz, 1H), 4.36 (t, *J* = 6.9 Hz,
511 2H), 3.98 (q, *J* = 7.1 Hz, 1H), 3.49 (s, 1H), 3.10 (t, *J* = 6.9 Hz, 2H), 1.95 (s, 1H), 1.17
512 (dt, *J* = 14.2, 6.8 Hz, 3H). ^{13}C NMR (101 MHz, DMSO) δ 160.60, 145.12, 144.80,
513 140.88, 139.09, 135.50, 131.56, 131.16, 130.56, 130.31, 128.36, 128.24, 127.47,
514 125.33, 125.16, 123.66, 122.39, 121.62, 120.36, 120.18, 118.15, 117.50, 112.97,
515 60.23, 41.38, 21.21, 19.33, 14.52. HRMS (ESI) m/z $[M + H]^+$: 511.1037 calcd for
516 $C_{24}H_{17}BrN_4O_3S$: 511.1039;

517 4.1.2.14. 3-[2-(trifluoromethoxy)benzenesulfonamide]-rutaecarpine (**6n**)

518 The intermediate **5** was treated with 2-(trifluoromethoxy)benzenesulfonyl chloride
519 according to the general procedure mentioned above to get compound **6n** as white

powder, in a yield of 61%; ^{1}H NMR (400 MHz, DMSO) δ 11.86 (s, 1H), 10.98 (s, 1H), 8.02 (d, *J* = 7.2 Hz, 1H), 7.88 – 7.73 (m, 2H), 7.68 – 7.52 (m, 5H), 7.46 (d, *J* = 8.3 Hz, 1H), 7.25 (t, *J* = 7.5 Hz, 1H), 7.08 (t, *J* = 7.4 Hz, 1H), 4.40 (t, *J* = 6.7 Hz, 2H), 3.37 (s, 1H), 3.15 (t, *J* = 6.7 Hz, 2H). ^{13}C NMR (101 MHz, DMSO) δ 160.61, 145.58, 144.97, 144.41, 139.07, 136.18, 135.42, 131.67, 131.49, 128.24, 128.09, 127.51, 127.23, 125.35, 125.14, 121.57, 121.57, 120.35, 120.18, 119.03, 118.07, 116.17, 112.96, 41.37, 19.33. HRMS (ESI) m/z $[M + H]^+$: 527.0987 calcd for $C_{24}H_{17}BrN_4O_3S$: 527.0988;

4.1.2.15. 3-[4-(trifluoromethoxy)benzenesulfonamide]-rutaecarpine (**6o**)

The intermediate **5** was treated with 4-(trifluoromethoxy)benzenesulfonyl chloride according to the general procedure mentioned above to get compound **6o** as white powder, in a yield of 54%; ^{1}H NMR (400 MHz, DMSO-D6) δ 11.81 (s, 1H), 10.75 (s, 1H), 7.85 (dd, *J* = 17.2, 5.6 Hz, 3H), 7.66 – 7.48 (m, 5H), 7.42 (d, *J* = 8.0 Hz, 1H), 7.21 (dd, *J* = 8.1, 7.2 Hz, 1H), 7.04 (t, *J* = 7.5 Hz, 1H), 4.36 (t, *J* = 6.8 Hz, 2H), 3.10 (t, *J* = 6.8 Hz, 2H). ^{13}C NMR (101 MHz, DMSO) δ 160.63, 145.15, 144.80, 143.60, 139.11, 135.36, 133.35, 133.03, 128.41, 128.15, 127.93, 127.49, 127.19, 127.19, 125.35, 125.17, 122.44, 121.68, 120.36, 120.19, 118.16, 117.19, 112.99, 41.39, 19.34. HRMS (ESI) m/z $[M + H]^+$: 527.0984 calcd for $C_{24}H_{17}BrN_4O_3S$: 527.0988;

4.1.2.16. 3-(4-acetylbenzenesulfonamide)-rutaecarpine (**6p**)

The intermediate **5** was treated with 4-acetylbenzenesulfonyl chloride according to the general procedure mentioned above to get compound **6p** as brown powder, in a yield of 48%; ^{1}H NMR (400 MHz, DMSO-D6) δ 11.80 (s, 1H), 10.81 (s, 1H), 8.06 (d, *J* = 8.2 Hz, 2H), 7.85 (dd, *J* = 17.5, 4.9 Hz, 3H), 7.63 – 7.46 (m, 3H), 7.41 (d, *J* = 8.3 Hz, 1H), 7.21 (t, *J* = 7.6 Hz, 1H), 7.03 (t, *J* = 7.5 Hz, 1H), 4.35 (t, *J* = 6.8 Hz, 2H), 3.10 (t, *J* = 6.8 Hz, 2H), 2.46 (s, 3H). ^{13}C NMR (101 MHz, DMSO) δ 197.68, 160.62, 145.05, 144.65, 143.26, 140.32, 139.07, 135.56, 129.62, 129.62, 128.35, 127.78, 127.52, 127.52, 125.33, 125.16, 121.62, 120.35, 120.18, 118.11, 116.94, 112.97, 41.37, 27.44, 27.44, 19.33. HRMS (ESI) m/z $[M + H]^+$: 485.1272 calcd for $C_{24}H_{17}BrN_4O_3S$:

485.1274;

4.1.2.17. 3-(2-thiophenesulfonamide)-rutaecarpine (**7a**)

The intermediate **5** was treated with 2-thiophenesulfonyl chloride according to the general procedure mentioned above to get compound **7a** as white powder, in a yield of 43%; ^{1}H NMR (400 MHz, DMSO-D6) δ 11.82 (s, 1H), 10.75 (s, 1H), 7.88 (s, 2H), 7.56 (dt, *J* = 14.8, 5.8 Hz, 4H), 7.42 (d, *J* = 8.3 Hz, 1H), 7.21 (t, *J* = 7.6 Hz, 1H), 7.12 – 7.00 (m, 2H), 4.38 (t, *J* = 6.7 Hz, 2H), 3.11 (t, *J* = 6.8 Hz, 2H), -0.10 (s, 4H). ^{13}C NMR (101 MHz, DMSO) δ 160.69, 145.07, 144.70, 140.05, 139.09, 135.75, 134.15, 133.06, 128.24, 128.24,127.96, 127.53, 125.36, 125.17, 121.59, 120.38, 120.20, 118.11, 117.09, 112.99, 41.40, 19.36. HRMS (ESI) m/z $[M + H]^+$: 449.0728 calcd for $C_{24}H_{17}BrN_4O_3S$: 449.0736;

4.1.2.18. 3-(5-bromothiophene-2-sulfonamide)-rutaecarpine (**7b**)

The intermediate **5** was treated with 5-bromothiophene-2-sulfonyl chloride according to the general procedure mentioned above to get compound **7b** as white powder, in a yield of 40%; ^{1}H NMR (400 MHz, DMSO-D6) δ 11.83 (s, 1H), 10.90 (s, 1H), 7.87 (d, *J* = 2.3 Hz, 1H), 7.66 – 7.51 (m, 3H), 7.42 (d, *J* = 8.3 Hz, 1H), 7.39 – 7.34 (m, 1H), 7.31 – 7.25 (m, 1H), 7.22 (t, *J* = 7.6 Hz, 1H), 7.05 (t, *J* = 7.5 Hz, 1H), 4.38 (t, *J* = 6.8 Hz, 2H), 3.12 (t, *J* = 6.7 Hz, 2H). ^{13}C NMR (101 MHz, DMSO) δ 160.68, 145.22, 144.96, 140.88, 139.11, 135.21, 133.77, 131.96, 128.40, 128.08, 127.50, 125.35, 125.19, 121.66, 120.38, 120.20, 119.86, 118.20, 117.37, 113.00, 41.42, 19.35. HRMS (ESI) m/z $[M + H]^+$: 528.9815 calcd for $C_{24}H_{17}BrN_4O_3S$: 528.9812;

4.1.2.19. 3-(5-chlorothiophene-2-sulfonamide)-rutaecarpine (**7c**)

The intermediate **5** was treated with 5-chlorothiophene-2-sulfonyl chloride according to the general procedure mentioned above to get compound **7c** as pale brown powder, in a yield of 37%; ^{1}H NMR (400 MHz, DMSO-D6) δ 11.83 (s, 1H), 10.91 (s, 1H), 7.88 (d, *J* = 2.3 Hz, 1H), 7.67 – 7.53 (m, 3H), 7.47 – 7.38 (m, 2H), 7.25

– 7.14 (m, 2H), 7.04 (t, *J* = 7.5 Hz, 1H), 4.38 (t, *J* = 6.8 Hz, 2H), 3.11 (t, *J* = 6.8 Hz, 2H). ^{13}C NMR (101 MHz, DMSO) δ 160.67, 145.23, 145.00, 139.11, 138.27, 135.94, 135.17, 133.04, 128.61, 128.40, 128.16, 127.50, 125.35, 125.19, 121.65, 120.38, 120.20, 118.21, 117.48, 112.99, 41.41, 19.35. HRMS (ESI) m/z $[M + H]^+$: 483.0343 calcd for $C_{24}H_{17}BrN_4O_3S$: 483.0346;

4.1.2.20. 3-(2-carbomethoxy-3-thiophenesulfonamide)-rutaecarpine (**8a**)

The intermediate **5** was treated with 2-carbomethoxy-3-thiophenesulfonyl chloride according to the general procedure mentioned above to get compound **8a** as white powder, in a yield of 36%; ^{1}H NMR (400 MHz, DMSO-D6) δ 11.80 (s, 1H), 10.51 (s, 1H), 7.94 (d, *J* = 5.3 Hz, 1H), 7.83 (d, *J* = 2.1 Hz, 1H), 7.55 (dt, *J* = 8.9, 5.6 Hz, 3H), 7.48 – 7.38 (m, 2H), 7.20 (t, *J* = 7.6 Hz, 1H), 7.03 (t, *J* = 7.5 Hz, 1H), 4.36 (t, *J* = 6.8 Hz, 2H), 3.31 (s, 1H), 3.10 (t, *J* = 6.8 Hz, 2H). ^{13}C NMR (101 MHz, DMSO) δ 160.65, 160.34, 144.93, 144.34, 142.56, 139.07, 135.66, 133.22, 132.68, 131.05, 128.22, 127.53, 127.25, 125.36, 125.12, 121.60, 120.34, 120.18, 118.03, 116.19, 112.97, 53.73, 41.38, 19.35. HRMS (ESI) m/z $[M + H]^+$: 507.0784 calcd for $C_{24}H_{17}BrN_4O_3S$: 507.0785;

4.2. AChE and BuChE inhibition assay

The ChE inhibition activity of the test compounds was performed adopting the method of Ellman et al. with modification. Acetylcholinesterase (AChE, C3389-2KU, from *electric eel*) was purchased from SigmaAldrich. Butylcholinesterase (BuChE, B128570-2KU, from *equine serum*), 5,5-dithiobis-(2-nitrobenzoic acid) (DTNB, Ellman's reagent, D105559-1g), acetylthiocholine iodide (ATCI, A100869-1g), S-Butyrylthiocholine iodide (BTCI, B100871-1g) and donepezil hydrochloride (D129948-1g) was obtained from Aladdin. Tacrine and donepezil were used as reference drugs. The compounds were dissolved in DMSO and then diluted in 0.1 M pH 8 phosphate buffer to provide different concentration (DMSO 0.1%). Briefly, 50μL DTNB, 10 μL of AChE or BuChE

(2U/ml), 10 μL different concentration of the test or standard compounds and 430 μL phosphate buffer were preincubated in 48-well plates at 37℃ for 30 min. Further, 50 μL the substrate ATCI or BTCI was added. The mixture was incubated for additional 30 min. Changes in absorbance were measured at 412 nm in a Biotek Synergy HTX Multi-Mode reader. To determine the IC_{50} (concentration of the compound resulting in 50% inhibition of the enzyme activity), log inhibitor concentration versus percent of inhibition curve was analyzed.

4.3. Kinetic characterization of BuChE inhibition

Enzyme kinetic studies was done in a similar manner as enzyme inhibition assay. Substrate (BTCI) in the presence of different concentrations of inhibitor (0−8μM) were measured at different times to determine the inhibition model and reciprocal plots of 1/V versus 1/[S].

4.4. Molecular modeling and dynamic simulation

The *Discovery Studio 2017 R2* (DS, BIOVIA Software, Inc., San Diego,CA, United States) was applied for molecular docking to gain the interaction between ligands and receptors. The X-ray crystal structure of the BuChE (PDB ID: 5NN0, co-crystallized with 92H) was obtained from Protein Data Bank. The structure of BuChE derived from the complex 5NN0 was prepared by removal of the original ligand and water molecules, and all polar hydrogen and CHARMm force fields were then added. And the treated protein was prepared using *Prepare Protein* protocol. The ligand was processed by *Full Minimization* of the *Small Molecular* protocol. Then the ligand was docked into the active site of protein using the *CDOCKER* program with default parameters. The docked conformation with the highest score of -*CDOCKER_INTERACTION_ENERGY* values was selected and analyzed.

MD simulations in explicit solvent water were performed. The system was minimized with fixed positions for all heavy atoms of BuChE and compound **6n** for

1,000 steps. And the system was gradually heated to 300 K during 100 ps. The equilibration process was started with a 100 ps simulation at 300K, while keeping all the heavy atoms of BuChE and compound **6n** fixed. This was followed by unconstrained minimization consisting of 1,000 steps. The production simulations were performed for 10000 ps with a 2 fs time step. Therefore, a 10000 ps dynamic calculation was performed in the NTP ensemble, with pressure constant at 1 atm and temperature constant at 300 K. RMSD properties of molecular dynamics trajectories was analyzed by *Analyze Trajectory* procedure.

4.5. Radical scavenging activity (DPPH assay)

The antioxidant capacity of the test compounds were evaluated by DPPH method in which DPPH free radical chould be scavenged by antioxidant. Brefly, 150 μL of the compound (100 μM) with 150 uL of DPPH (140 μM) was mixed and incubated in a 96-well plate for 2 hours in the dark at 37 °C. The relevant absorbance of the reaction mixture was measured at 520 nm using a microplate reader (BioTek Synergy HT). The reducing percentage (RP) of DPPH was determined by the formula : $RP = (1 - A_c/A_0) \times 100\%$, where A_c/A_0 are DPPH absorbance in the presence and absence of inhibitors, respectively. Ascorbic acid was used as a standard for DPPH determination.

4.6. Determination of the intracellular ROS production

Intracellular ROS production can cause oxidative stress and accelerate the progression of neurodegenerative diseases. 2', 7' - dichlorofluorescein diacetate (DCFH-DA) assay was applied to determine ROS formation. Briefly, SH-SY5Y cells were seeded in 96-well plates (1×10^4 cells per well) and incubated at 37 ° C containing 5% CO_2 for 24 hours. After cells being incubated in the presence or absence of different concentrations of the test compound for 6 hours, the cells were washed with PBS. Then the cells were exposed to H_2O_2 (250 μM) or Aβ (5 μM) for 24 hours. The cells were washed with PBS again and incubated with DCFH-DA (10 μM)

for 1h in the dark. At the end of the incubation, DCFH-DA was removed. The fluorescence intensity of the dichlorofluorescein (DCF) from the cells was measured at 488 nm excitation and 525 nm emission wavelengths using Synergy HTX fluorescence microplate reader. Results were expressed as the percentage of intracellular ROS compared to untreated control cells.

4.7. Effect on Aβ peptide aggregation

Aggregation of Aβ peptide in brain was considered to be an inportant factor of the pathogenesis of AD. Inhibition of self-induced Aβ aggregation was investigated using thioflavin T (ThT) fluorescence assay as described. Aβ(1-42) peptide (MB10425, Meilun Biotechnology Co., LTD) was prepared in phosphate buffer (pH 7.4) containing 1% ammonium hydroxide. The test compound was prepared in DMSO to obtain a 10 mM solution and diluted further with phosphate buffer. Briefly, 10 μL of Aβ(1-42) was incubated in the absence and presence of 10 μL of the test compound to obtain final concentration of 20 μM Aβ(1–42) and 100 μM the test compound. The mixture was incubated at room temperature. After 48 h incubation, 5 μM ThT (prepared in 50 mM glycine-NaOH buffer; pH 8.5) was added to make the volume of 200 μL. Fluorescence intensity of the solution was measured at 450 nm excitation and 485 nm emission wavelengths using Synergy HTX fluorescence microplate reader. The percentage inhibition of the self-induced Aβ(1–42) aggregation for the test compound was calculated by the following formula: $(1 - IF_i / If_o) \times 100\%$, in which IF_i and IF_o are fluorescence intensities in the presence and absence of inhibitors, respectively.

4.8. Metal-chelating research

The metal binding property of the test compound was investigated using a UV-vis spectrophotometer with a wavelength range of 200-600 nm. The UV absorption of the selected compound (20 μM) in the absence and presence of $CuCl_2$, $FeSO_4$, $ZnCl_2$, $AlCl_3$, $MgCl_2$ and $CaCl_2$ (20 μM) was recorded in a 1 cm quartz cell for 1 hour. The

final volume of the reaction mixture was 2 mL. The molar ratio method was carried out to determine the stoichiometry of the complex. A solution of the test compound (20 μM) was titrated by a molar solution of increasing amount of $CuCl_2$.

4.9. Oil/water partition coefficient assay and ADMET prediction

Using the classical shake flask method, the oil/water partition coefficient of the compounds were tested. The same amount of oleic phase (noctanol) and aqueous phase (PBS pH 7.4) were mixed. And the mixture was shaken by ultrasonic (400 W, 40 kHz) and allowed to stand for 24 h to obtain a saturated solution of noctanol. An appropriate amount of the compounds was added. After sealing, the test compounds was shaken at 37 °C for 48 h to make it fully equilibrated in the two phases. Then the mixture was measured with an ultraviolet spectrophotometer.

The predictive ADMET pharmacokinetic properties, including human intestinal absorption (HIA), aqueous solubility, blood-brain-barrier penetration (BBB), cytochrome P450 2D6 (CYP2D6) enzyme inhibition, plasma protein binding (PPB) were analyzed quantitatively for the selected eight ligands using ADMET descriptors tools in *Discovery Studio 2017 R2*. The selected eight ligands were processed as described above and input to computer program. Parameters of ADMET prediction program were set in the normal mode.

4.10. Neuroprotection assay

4.10.1. Neuroprotective effects of all compounds against H_2O_2-induced PC12cell death

Viability of PC12 cell (rat adrenal chromaffin differentiated cell line) of all compounds against H_2O_2-induced cytotoxicity was detected by 3-(4,5-dimethylthiazol-2-yl)-2,5-diphenyl tetrazolium bromide (MTT) assay. PC12 cells were seeded in 96-well plates (1×10^4 cells per well) and incubated at 37 °C containing 5% CO_2. After 24 hours, cells were incubated with different concentrations

of the test compounds for 3 hours, then the cells were exposed with H_2O_2 (250 μM) for 24 hours. Cell viability was measured by MTT assay. Briefly, 20 mL of 0.5 mg/mL MTT reagent was added after removal of the previous medium and incubated for 4 h. After 4 h, the medium was removed and the crystal of the formazan was then dissolved 150 mL DMSO. The relevant absorbance was measured at 570 nm on the Biotek Synergy HTX Multi-Mode reader. Cell viability are expressed as the percentage of untreated control cells (PC12 cells in the absence of test compound and H_2O_2).

4.10.2. Neuroprotective test of the selected compound against H_2O_2 or Aβ-induced SH-SY5Y cell death

The Aβ(1-42) peptide was incubated in serum medium at a final concentration of 5 μM for 24 hours to induce Aβ aggregation for neuroprotective test. Neuroprotective test of the selected compound against H_2O_2 or Aβ-induced SH-SY5Y cell (human neuroblastoma cell) death was performed in a same manner as described above.

4.11. Statistical analysis

Data are reported as mean ± SEM of at least three independent experiments and data analysis was performed with GraphPad Prism 6 software.

Abbreviation

Alzheimer's disease (AD)
β-amyloid protein (Aβ)
Acetylcholinesterase (AChE)
Butyrylcholinesterase (BuChE)
Cholinesterase (ChE)
Reactive oxygen species (ROS)

Multitarget-directed ligands (MTDLs)

Rutaecarpine (Ru)

Tacrine (THA)

Studio Discovery 2017 R2 (DS)

Molecular dynamics (MD)

Root-mean-square deviation (RMSD)

1,1-Diphenyl-2-picrylhydrazyl (DPPH)

2',7'-Dichlorodihydrofluorescein diacetate (DCFH-DA)

Dichlorofluorescein (DCF)

Thioflavin T (Th T)

Transmission Electron Microscopy (TEM)

Absorption, distribution, metabolism, excretion, and toxicity (ADMET)

human intestinal absorption (HIA)

blood-brain-barrier penetration (BBB),

cytochrome P450 2D6 (CYP2D6)

plasma protein binding (PPB)

5,5-dithiobis-(2-nitrobenzoic acid) (DTNB)

acetylthiocholine iodide (ATCI)

S-Butyrylthiocholine iodide (BTCI)

3-(4,5-dimethylthiazol-2-yl)-2,5-diphenyl tetrazolium bromide (MTT)

Conflict of interest

We declare that we have no conflict of interest.

Acknowledgments

We thank the General Financial Grants from the China Postdoctoral Science Foundation (2015M571916), the National Nature Science Foundation of China (81302701)for financial support of this study.

References

[1] T.L. Emmerzaal, A.J. Kiliaan, D.R. Gustafson, 2003-2013: a decade of body mass index, Alzheimer's disease, and dementia, Journal of Alzheimer's disease : JAD, 43 (2015) 739-755.

[2] Y. Wu, Z. Li, Y.Y. Huang, D. Wu, H.B. Luo, Novel Phosphodiesterase Inhibitors for Cognitive Improvement in Alzheimer's Disease, Journal of medicinal chemistry, 61 (2018) 5467-5483.

[3] Q. Li, S. He, Y. Chen, F. Feng, W. Qu, H. Sun, Donepezil-based multi-functional cholinesterase inhibitors for treatment of Alzheimer's disease, European journal of medicinal chemistry, 158 (2018) 463-477.

[4] X. Du, X. Wang, M. Geng, Alzheimer's disease hypothesis and related therapies, Translational neurodegeneration, 7 (2018) 2.

[5] N.I. Bohnen, M.J. Grothe, N.J. Ray, M. Muller, S.J. Teipel, Recent advances in cholinergic imaging and cognitive decline-Revisiting the cholinergic hypothesis of dementia, Current geriatrics reports, 7 (2018) 1-11.

[6] G. Mushtaq, N.H. Greig, J.A. Khan, M.A. Kamal, Status of acetylcholinesterase and butyrylcholinesterase in Alzheimer's disease and type 2 diabetes mellitus, CNS & neurological disorders drug targets, 13 (2014) 1432-1439.

[7] M.M. Mesulam, A. Guillozet, P. Shaw, A. Levey, E.G. Duysen, O. Lockridge, Acetylcholinesterase knockouts establish central cholinergic pathways and can use butyrylcholinesterase to hydrolyze acetylcholine, Neuroscience, 110 (2002) 627-639.

[8] J. Hroudova, N. Singh, Z. Fisar, K.K. Ghosh, Progress in drug development for Alzheimer's disease: An overview in relation to mitochondrial energy metabolism, European journal of medicinal chemistry, 121 (2016) 774-784.

[9] P.B. Watkins, H.J. Zimmerman, M.J. Knapp, S.I. Gracon, K.W. Lewis, Hepatotoxic effects of tacrine administration in patients with Alzheimer's disease, The journal of the american medical association, 271 (1994) 992-998.

[10] D.B. Hogan, C. Patterson, Progress in clinical neurosciences: Treatment of Alzheimer's disease and other dementias-review and comparison of the cholinesterase inhibitors, Canadian journal of neurological sciences, 29 (2002) 306-314.

[11] Y. Furukawa-Hibi, T. Alkam, A. Nitta, A. Matsuyama, H. Mizoguchi, K. Suzuki, S. Moussaoui, Q.S. Yu, N.H. Greig, T. Nagai, K. Yamada, Butyrylcholinesterase inhibitors ameliorate cognitive dysfunction induced by amyloid-beta peptide in mice, Behavioural brain research, 225 (2011) 222-229.

[12] Q. Li, H. Yang, Y. Chen, H. Sun, Recent progress in the identification of selective butyrylcholinesterase inhibitors for Alzheimer's disease, European journal of medicinal chemistry, 132 (2017) 294-309.

[13] S. Sadigh-Eteghad, B. Sabermarouf, A. Majdi, M. Talebi, M. Farhoudi, J. Mahmoudi, Amyloid-beta: a crucial factor in Alzheimer's disease, Medical principles and practice : international journal of the Kuwait University, Health Science Centre, 24 (2015) 1-10.

[14] P. Salahuddin, M.T. Fatima, A.S. Abdelhameed, S. Nusrat, R.H. Khan, Structure of amyloid oligomers and their mechanisms of toxicities: Targeting amyloid oligomers using novel therapeutic approaches, in: European journal of medicinal chemistry, 2016, pp. 41-58.

[15] M. Marttinen, M. Takalo, T. Natunen, R. Wittrahm, S. Gabbouj, S. Kemppainen, V. Leinonen, H. Tanila, A. Haapasalo, M. Hiltunen, Molecular Mechanisms of Synaptotoxicity and Neuroinflammation in Alzheimer’s Disease, Frontiers in Neuroscience, 12 (2018).

[16] C. Cheignon, M. Tomas, D. Bonnefont-Rousselot, P. Faller, C. Hureau, F. Collin, Oxidative stress and the amyloid beta peptide in Alzheimer's disease, Redox biology, 14 (2018) 450-464.

[17] T.M. Florence, The role of free radicals in disease, Australian and New Zealand journal of ophthalmology, 23 (1995) 3-7.

[18] M.G. Savelieff, A.S. DeToma, J.S. Derrick, M.H. Lim, The ongoing search for small molecules to study metal-associated amyloid-beta species in Alzheimer's disease, Accounts of chemical research, 47 (2014) 2475-2482.

[19] B.X. Wong, Y.H. Hung, A.I. Bush, J.A. Duce, Metals and cholesterol: two sides of the same coin in Alzheimer's disease pathology, Frontiers in aging neuroscience, 6 (2014) 91.

[20] M.M. Ibrahim, M.T. Gabr, Multitarget therapeutic strategies for Alzheimer's disease, Neural regeneration research, 14 (2019) 437-440.

[21] A. Agis-Torres, M. Solhuber, M. Fernandez, J.M. Sanchez-Montero, Multi-Target-Directed Ligands and other Therapeutic Strategies in the Search of a Real Solution for Alzheimer's Disease, Current neuropharmacology, 12 (2014) 2-36.

[22] Y. Zhang, T. Yan, D. Sun, C. Xie, Y. Zheng, L. Zhang, T. Yagai, K.W. Krausz, W.H. Bisson, X. Yang, F.J. Gonzalez, Structure-Activity Relationships of the Main Bioactive Constituents of Euodia rutaecarpa on Aryl Hydrocarbon Receptor Activation and Associated Bile Acid Homeostasis, Drug metabolism and disposition: the biological fate of chemicals, 46 (2018) 1030-1040.

[23] J.K. Son, H.W. Chang, Y. Jahng, Progress in Studies on Rutaecarpine. II.--Synthesis and Structure-Biological Activity Relationships, Molecules, 20 (2015) 10800-10821.

[24] S. Jia, C. Hu, Pharmacological effects of rutaecarpine as a cardiovascular protective agent, Molecules, 15 (2010) 1873-1881.

[25] K. Chand, Rajeshwari, E. Candeias, S.M. Cardoso, S. Chaves, M.A. Santos, Tacrine-deferiprone hybrids as multi-target-directed metal chelators against Alzheimer's disease: a two-in-one drug, Metallomics : integrated biometal science, 10 (2018) 1460-1475.

[26] B. Wang, Y.C. Mai, Y. Li, J.Q. Hou, S.L. Huang, T.M. Ou, J.H. Tan, L.K. An, D. Li, L.Q. Gu, Z.S. Huang, Synthesis and evaluation of novel rutaecarpine derivatives and related alkaloids derivatives as selective acetylcholinesterase inhibitors, European journal of medicinal chemistry, 45 (2010) 1415-1423.

[27] Y. He, P.F. Yao, S.B. Chen, Z.H. Huang, S.L. Huang, J.H. Tan, D. Li, L.Q. Gu, Z.S. Huang, Synthesis and evaluation of 7,8-dehydrorutaecarpine derivatives as potential multifunctional agents for the treatment of Alzheimer's disease, European journal of medicinal chemistry, 63 (2013) 299-312.

[28] Z. Li, B. Wang, J.Q. Hou, S.L. Huang, T.M. Ou, J.H. Tan, L.K. An, D. Li, L.Q. Gu, Z.S. Huang, 2-(2-indolyl-)-4(3H)-quinazolines derivates as new inhibitors of AChE: design, synthesis, biological evaluation and molecular modelling, Journal of enzyme inhibition and medicinal chemistry, 28 (2013) 583-592.

[29] U. Kosak, B. Brus, D. Knez, R. Sink, S. Zakelj, J. Trontelj, A. Pislar, J. Slenc, M. Gobec, M. Zivin, L. Tratnjek, M. Perse, K. Salat, A. Podkowa, B. Filipek, F. Nachon, X. Brazzolotto, A. Wieckowska, B. Malawska, J. Stojan, I.M. Rascan, J. Kos, N. Coquelle, J.P. Colletier, S. Gobec, Development of an in-vivo active reversible butyrylcholinesterase inhibitor, Scientific reports, 6 (2016) 39495.

[30] U. Kosak, B. Brus, D. Knez, S. Zakelj, J. Trontelj, A. Pislar, R. Sink, M. Jukic, M. Zivin, A. Podkowa, F. Nachon, X. Brazzolotto, J. Stojan, J. Kos, N. Coquelle, K. Salat, J.P. Colletier, S. Gobec, The Magic of Crystal Structure-Based Inhibitor Optimization: Development of a Butyrylcholinesterase Inhibitor with Picomolar Affinity and in Vivo Activity, Journal of medicinal chemistry, 61 (2018) 119-139.

[31] J. Reis, F. Cagide, M.E. Valencia, J. Teixeira, D. Bagetta, C. Perez, E. Uriarte, P.J. Oliveira, F. Ortuso, S. Alcaro, M.I. Rodriguez-Franco, F. Borges, Multi-target-directed ligands for Alzheimer's disease: Discovery of chromone-based monoamine oxidase/cholinesterase inhibitors, European journal of medicinal chemistry, 158 (2018) 781-800.

[32] X. Li, H. Wang, Z. Lu, X. Zheng, W. Ni, J. Zhu, Y. Fu, F. Lian, N. Zhang, J. Li, H. Zhang, F. Mao, Development of Multifunctional Pyrimidinylthiourea Derivatives as Potential Anti-Alzheimer Agents, Journal of

847 medicinal chemistry, 59 (2016) 8326-8344.
848 [33] J. Bergman, S. Bergman, Studies of rutaecarpine and related quinazolinocarboline alkaloids, The Journal of
849 Organic Chemistry, 50 (1985) 1246-1255.
850 [34] J. Das, M. Sitaram Kumar, D. Subrahmanyam, T.V. Sastry, C. Prasad Narasimhulu, C.V. Laxman Rao, M.
851 Kannan, M. Roshaiah, R. Awasthi, S.N. Patil, H.M. Sarnaik, N.V. Rao Mamidi, N. Selvakumar, J. Iqbal,
852 Substituent activity relationship studies on new azolo benzoxazepinyl oxazolidinones, Bioorganic & medicinal
853 chemistry, 14 (2006) 8032-8042.
854 [35] B. Li, A.L. Huang, Y.L. Zhang, Z. Li, H.W. Ding, C. Huang, X.M. Meng, J. Li, Design, Synthesis and
855 Evaluation of Hesperetin Derivatives as Potential Multifunctional Anti-Alzheimer Agents, Molecules, 22 (2017).
856 [36] B. Brus, U. Kosak, S. Turk, A. Pislar, N. Coquelle, J. Kos, J. Stojan, J.P. Colletier, S. Gobec, Discovery,
857 biological evaluation, and crystal structure of a novel nanomolar selective butyrylcholinesterase inhibitor, Journal
858 of medicinal chemistry, 57 (2014) 8167-8179.
859 [37] L. Zhang, L. Fu, S. Zhang, J. Zhang, Y. Zhao, Y. Zheng, G. He, S. Yang, L. Ouyang, B. Liu, Discovery of a
860 small molecule targeting ULK1-modulated cell death of triple negative breast cancer in vitro and in vivo,
861 Chemical science, 8 (2017) 2687-2701.
862 [38] B.D. Freudenthal, W.A. Beard, L. Perera, D.D. Shock, T. Kim, T. Schlick, S.H. Wilson, Uncovering the
863 polymerase-induced cytotoxicity of an oxidized nucleotide, Nature, 517 (2015) 635-639.
864 [39] S. Vijayakumar, P. Manogar, S. Prabhu, R.A. Sanjeevkumar Singh, Novel ligand-based docking; molecular
865 dynamic simulations; and absorption, distribution, metabolism, and excretion approach to analyzing potential
866 acetylcholinesterase inhibitors for Alzheimer's disease, Journal of pharmaceutical analysis, 8 (2018) 413-420.
867 [40] S.B. Kedare, R.P. Singh, Genesis and development of DPPH method of antioxidant assay, Journal of food
868 science and technology, 48 (2011) 412-422.
869 [41] N. Yassa, H.R. Beni, A. Hadjiakhoondi, Free radical scavenging and lipid peroxidation activity of the Shahani
870 black grape, Pakistan journal of biological sciences : PJBS, 11 (2008) 2513-2516.
871 [42] Z. Chen, C. Zhong, Oxidative stress in Alzheimer's disease, Neuroscience bulletin, 30 (2014) 271-281.
872 [43] M. Baeeri, S. Momtaz, M. Navaei-Nigjeh, K. Niaz, M. Rahimifard, S.F. Ghasemi-Niri, N. Sanadgol, M.
873 Hodjat, M. Sharifzadeh, M. Abdollahi, Molecular evidence on the protective effect of ellagic acid on
874 phosalone-induced senescence in rat embryonic fibroblast cells, Food and chemical toxicology : an international
875 journal published for the British Industrial Biological Research Association, 100 (2017) 8-23.
876 [44] Y. Yang, M. Cui, Radiolabeled bioactive benzoheterocycles for imaging beta-amyloid plaques in Alzheimer's
877 disease, European journal of medicinal chemistry, 87 (2014) 703-721.
878 [45] K. Czarnecka, N. Chufarova, K. Halczuk, K. Maciejewska, M. Girek, R. Skibinski, J. Jonczyk, M. Bajda, J.
879 Kabzinski, I. Majsterek, P. Szymanski, Tetrahydroacridine derivatives with dichloronicotinic acid moiety as
880 attractive, multipotent agents for Alzheimer's disease treatment, European journal of medicinal chemistry, 145
881 (2018) 760-769.
882 [46] J. Cen, H. Guo, C. Hong, J. Lv, Y. Yang, T. Wang, D. Fang, W. Luo, C. Wang, Development of
883 tacrine-bifendate conjugates with improved cholinesterase inhibitory and pro-cognitive efficacy and reduced
884 hepatotoxicity, European journal of medicinal chemistry, 144 (2018) 128-136.
885 [47] S.Y. Chen, Y. Chen, Y.P. Li, S.H. Chen, J.H. Tan, T.M. Ou, L.Q. Gu, Z.S. Huang, Design, synthesis, and
886 biological evaluation of curcumin analogues as multifunctional agents for the treatment of Alzheimer's disease,
887 Bioorganic & medicinal chemistry, 19 (2011) 5596-5604.
888 [48] M.G. Savelieff, S. Lee, Y. Liu, M.H. Lim, Untangling amyloid-beta, tau, and metals in Alzheimer's disease,
889 ACS chemical biology, 8 (2013) 856-865.
890 [49] D.M. Miller, G.R. Buettner, S.D. Aust, Transition metals as catalysts of "autoxidation" reactions, Free radical

biology & medicine, 8 (1990) 95-108.
[50] L. Di, E.H. Kerns, I.F. Bezar, S.L. Petusky, Y. Huang, Comparison of blood-brain barrier permeability assays: in situ brain perfusion, MDR1-MDCKII and PAMPA-BBB, Journal of pharmaceutical sciences, 98 (2009) 1980-1991.
[51] P.A. Nogara, A. Saraiva Rde, D. Caeran Bueno, L.J. Lissner, C. Lenz Dalla Corte, M.M. Braga, D.B. Rosemberg, J.B. Rocha, Virtual screening of acetylcholinesterase inhibitors using the Lipinski's rule of five and ZINC databank, BioMed research international, 2015 (2015) 870389.
[52] D.G. Levitt, Quantitative relationship between the octanol/water partition coefficient and the diffusion limitation of the exchange between adipose and blood, BMC clinical pharmacology, 10 (2010) 1.
[53] J. Grover, V. Kumar, V. Singh, K. Bairwa, M.E. Sobhia, S.M. Jachak, Synthesis, biological evaluation, molecular docking and theoretical evaluation of ADMET properties of nepodin and chrysophanol derivatives as potential cyclooxygenase (COX-1, COX-2) inhibitors, European journal of medicinal chemistry, 80 (2014) 47-56.
[54] L. Jalili-Baleh, H. Forootanfar, T.T. Kucukkilinc, H. Nadri, Z. Abdolahi, A. Ameri, M. Jafari, B. Ayazgok, M. Baeeri, M. Rahimifard, S.N. Abbas Bukhari, M. Abdollahi, M.R. Ganjali, S. Emami, M. Khoobi, A. Foroumadi, Design, synthesis and evaluation of novel multi-target-directed ligands for treatment of Alzheimer's disease based on coumarin and lipoic acid scaffolds, European journal of medicinal chemistry, 152 (2018) 600-614.

Figure and table legends：

Figure 1. Design of the target BuChE inhibitor compounds. (A) Structures of rutaecarpine (**Ru**) and tacrine (**THA**). (B) Structure of the sulfonamide BuChE inhibitor reported in the literature. (C) Structure of the target benzenesulfonylamino-substituted and thiazolesulfonamide-substituted **Ru** derivatives.

Figure 2. Lineweaver–Burk plot obtained through the kinetics study of the inhibitory effects of compound **6n** on BuChE**.** Reciprocals of enzyme activity (BuChE) versus reciprocals of the substrate (butyrylthiocholine iodide) in the presence of different concentration of compound **6n**.

Figure 3. (A) 3D mode of the H bond surface of compound **6n** with receptor BuChE (PDB ID: 5NN0). (B) 2D mode of the interaction of compound **6n** with receptor BuChE (conventional H bond and C–H bond, halogen, π–cation, alkyl, and π–alkyl are represented by green, light green, blue, yellow, pink, and light pink lines, respectively).

Figure 4. Root mean square deviation (RMSD) vs. time.

Figure 5. Potency of compound **6n** as a promising neuroantioxidant for reducing the formation of intracellular ROS in SH-SY5Y and PC12 cells. Results are presented as the mean ± SEM of three independent experiments (##$P < 0.01$ versus control group; ***$P < 0.001$, **$P < 0.01$, *$P < 0.05$ versus H_2O_2 group).

Figure 6. TEM images showing the self-induced aggregation of 5 μM Aβ (1-42) in the presence or absence of compounds. (A) Aβ (1-42) incubated alone at 0 h, (B) Aβ (1-42) incubated alone at 48 h, (C) Aβ (1-42) incubated with 100 μM compound **6n** at 48 h, (D) Aβ(1-42) incubated with 100 μM donepezil at 48 h.

Figure 7. (A) UV spectrum of compound **6n** (20 μM) alone or mixed with $CuCl_2$, $FeSO_4$, $ZnCl_2$, $AlCl_3$, $MgCl_2$, and $CaCl_2$ (20 μM). (B) Determination of the stoichiometry of Cu^{2+}/**6n** complex through the molar ratio method.

Figure 8. Regression based on ADMET_PSA_2D and ADMET_AlogP98. The compound set lies entirely within the 95% confidence ellipse. (Red and green ellipses described 95% and 99% of HIA, respectively; the pink and sky blue ellipses described 95% and 99% of BBB, respectively).

Figure 9. Neuroprotective potency of compound **6n** against cytotoxicity toward human neuroblastoma SH-SY5Y cells. (A) H_2O_2–induced group. (B) Aβ–induced group. Results are expressed as the mean ± SEM of three independent experiments, ###P < 0.001 compared with the control group; ***P < 0.001 compared with the H_2O_2 or Aβ group.

Table 1. In vitro ChE inhibitory activity and free radical scavenging rate of the synthesized derivatives.

Table 2. Inhibitory rate of compound **6n** for self-mediated Aβ aggregation.

Table 3. Log P values of active compounds.

Table 4. ADMET properties of active compounds.

Table 5. Neuroprotective effects of synthesized rutacecarpine derivatives against H_2O_2-induced cytotoxicity toward PC12 cells.

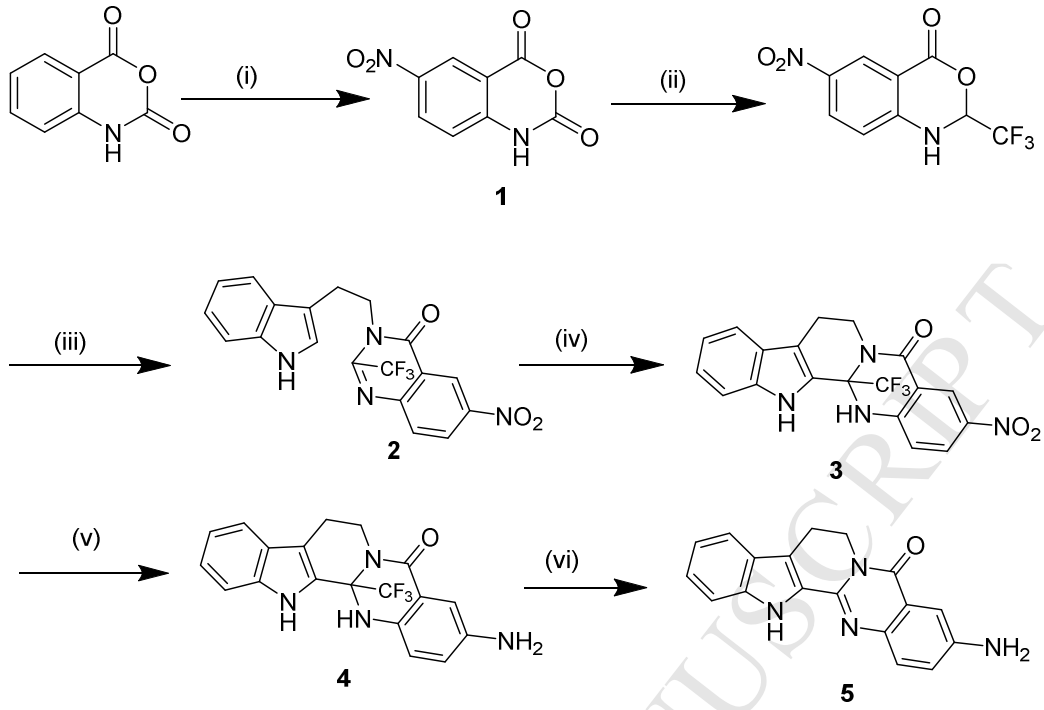

949

950 **Scheme 1.** Synthesis of intermediate 3-amino-substituted **Ru** in accordance with the modified
951 Bergman procedure. Reagents and conditions: (i) concentrated H_2SO_4, KNO_3, 0°C;(ii) $(CF_3CO)_2O$,
952 pyridine, 25°C, 30 min; (iii) tryptamine, reflux, 3 h; (iv) HCI, AcOH, reflux, 1 h; (v) 10% Pd/C,
953 80% hydrazine hydrate, isopropanol, 80°C, reflux, 1 h; (vi) KOH, H_2O, EtOH, reflux, 30 min.

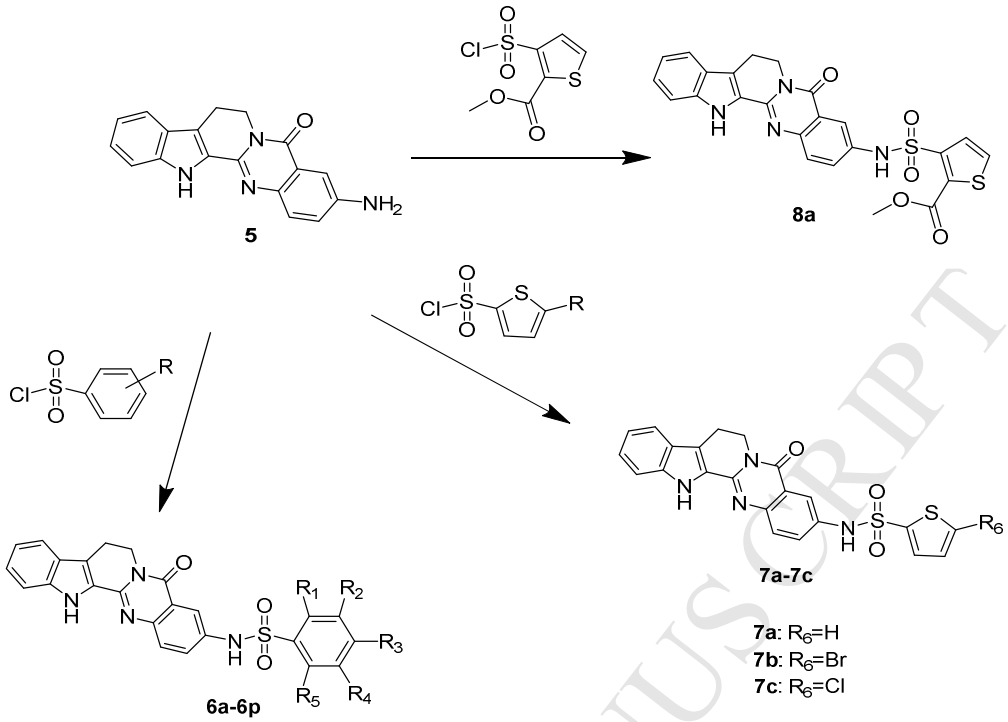

6a: R_1=R_2=R_4=R_5=H, R_3=OCH_3
6b: R_2=R_4=R_5=H, R_1=R_3=OCH_3
6c: R_1=R_4=R_5=H, R_2=R_3=OCH_3
6d: R_1=R_2=R_4=R_5=H, R_3=NO_2
6e: R_1=R_3=R_4=R_5=H, R_2=NO_2
6f: R_1=R_2=R_4=R_5=H, R_3=Br
6g: R_2=R_3=R_4=H, R_1=R_5=Cl
6h: R_1=R_3=R_5=H, R_2=R_4=Cl
6i: R_1=R_4=R_5=H, R_2=Cl, R_3=F
6j: R_1=R_2=R_4=R_5=H, R_3=$C(CH_3)_3$
6k: R_1=R_2=R_4=R_5=H, R_3=F
6l: R_1=R_2=R_4=R_5=H, R_3=CF_3
6m: R_1=R_3=R_4=R_5=H, R_2=CF_3
6n: R_2=R_3=R_4=R_5=H, R_1=OCF_3
6o: R_1=R_2=R_4=R_5=H, R_3=OCF_3
6p: R_1=R_2=R_4=R_5=H, R_3=$COCH_3$

7a: R_6=H
7b: R_6=Br
7c: R_6=Cl

Scheme 2. Synthesis of 3-aminoalkanamido-substituted **Ru** derivatives. Reagents and conditions: pyridine, reflux, 30 min.

Table 1. In vitro ChE inhibitory activity and free radical scavenging rate of the synthesized derivatives.

Compounds	AChE Inhibition, (IC50) μM[a]	BuChE Inhibition, (IC50) μM[a]	SI[b]	RP of DPPH assay[c]
Ru	>100	>100	nd[d]	nd[d]
6a	>100	8.01 ± 1.54	>12.5	45.50 ± 4.61
6b	77.02 ± 5.04	7.58 ± 1.07	>10.2	43.74 ± 5.74
6c	51.24 ± 3.74	10.90 ± 1.39	4.7	40.31 ± 2.87
6d	>100	16.51 ± 1.64	>6.1	35.18 ± 3.02
6e	>100	23.32 ± 1.49	>4.3	40.25 ± 1.53
6f	40.43 ± 2.46	8.94 ± 1.85	4.5	59.07 ± 4.62
6g	100	13.65 ± 1.60	>7.3	55.94 ± 3.86
6h	84.37 ± 4.52	7.94 ± 1.26	10.6	53.68 ± 3.26
6i	85.61 ± 4.98	4.63 ± 0.74	18.5	58.03 ± 4.68
6j	>100	12.95 ± 1.25	>7.8	37.23 ± 2.39
6k	>100	7.57 ± 0.77	>13.2	55.79 ± 6.40
6l	>100	8.28 ± 0.91	>12.1	59.32 ± 4.60
6m	>100	3.82 ± 0.68	>26.2	54.28 ± 3.57
6n	>100	3.60 ± 0.34	>28.8	57.57 ± 5.82
6o	34.56 ± 3.19	3.95 ± 0.72	8.7	53.49 ± 2.35
6p	>100	25.78 ± 1.31	>3.9	48.01 ± 4.54
7a	>100	>100	nd[d]	41.76 ± 3.87
7b	83.36 ± 5.17	60.34 ± 4.03	1.4	56.35 ± 5.81
7c	>100	76.93 ± 4.95	>1.3	44.95 ± 4.13
8a	>100	>100	nd[d]	44.54 ± 3.78
THA	0.28 ± 0.026	0.04 ± 0.007	7.0	53.62 ± 4.77
Donepezil	0.02 ± 0.01	7.87 ± 1.24	0.003	81.89 ± 7.35
Ascorbic acid	nd[d]	nd[d]	nd[d]	70.57 ± 5.51

[a]AChE from electric eel and BuChE from equine serum were used. IC_{50}, 50% inhibitor concentration values are expressed as the mean ± SEM of the three experiments. [b]Selectivity ratio = (IC_{50} of AChE)/(IC_{50} of BuChE). [c]RP of 1, 1-Diphenyl-2-picrylhydrazyl (DPPH) (%) = reduction percentage of DPPH, compounds at a concentration of 100 μM. [d]nd = not determined.

Table 2. Inhibitory rate of compound **6n** for self-mediated Aβ aggregation.

Compounds	Inhibition of self-induced Aβ aggregation (%) [a]
Ru	11.25 ± 1.9
6n	58.95 ± 4.0
Donepezil	33.78 ± 4.5

[a] Inhibition of the self-induced aggregation of 5 μM Aβ in the presence of 100 μM Ru, **6n**, or donepezil. Results are expressed as the mean ± SEM of the three independent experiments.

Table 3. Log P values of active compounds.

Compounds	Log P[a]
6k	2.25
6l	3.01
6h	3.21
6m	3.01
6n	3.62
6i	2.81
6o	3.62
7b	2.91

[a] Apparent oil/water partition coefficient.

Table 4. ADMET properties of active compounds.

Compounds	A[a]	D[b]		M[c]	E[d]	AlogP98[e]	PSA2D[f]
6k	0	1	2	0	1	4.006	79.388
6l	0	2	3	0	2	2.848	92.198
6h	0	2	2	0	2	3.463	79.388
6m	0	2	2	0	1	3.595	81.416
6n	0	1	2	0	1	3.968	79.388
6i	0	2	3	0	1	2.479	92.198
6o	0	2	2	0	2	3.094	79.388
7b	0	2	2	0	1	3.226	81.416

[a] Absorption: Intestinal absorption.

[b] Distribution: Aqueous solubility and blood-brain barrier penetration.

[c] Metabolism: CYPA2D6.

[d] Excretion: Plasma protein binding.

[e] ALogP98: Predicted octanol/water.

[f] PSA: polar surface area, 2D: two-dimensional.

Table 5. Neuroprotective effects of synthesized rutacecarpine derivatives against H_2O_2-induced cytotoxicity toward PC12 cells.

Compounds	PC12 Cell viability(% of control)[a]					
	H_2O_2	1 μM	5 μM	10 μM	30 μM	50 μM
6a	37.35 ± 3.87	39.31 ± 4.24	51.84 ± 1.23	42.27 ± 3.01	43.25 ± 3.63	49.04 ± 2.05
6b	45.06 ± 2.46	49.64 ± 4.57	51.07±5.14	51.95 ± 3.59	56.02 ± 5.25	51.12 ± 3.36
6c	38.01 ± 1.94	40.43 ± 3.61	43.98 ± 2.09	45.18 ± 3.16	47.72 ± 3.04	50.95 ± 6.03
6d	48.16 ± 5.14	32.42 ± 2.08	33.03 ± 2.08	37.09 ± 1.56	33.53 ± 1.23	30.96 ± 4.65
6e	43.16 ± 1.66	27.04± 5.02	38.67 ± 5.01	40.91 ± 3.03	34.02 ± 2.02	25.63 ± 3.23
6f	37.35 ± 2.41	39.94 ± 4.55	41.83 ± 4.09	44.13 ± 1.59	45.41 ± 1.07	47.62 ± 1.61
6g	38.01 ± 6.93	40.73 ± 1.66	42.11 ± 1.03	42.89 ± 4.19	45.43 ± 2.02	48.32 ± 3.06
6h	40.06 ± 3.56	42.43 ± 4.94	45.33± 2.23	47.94 ± 5.19	59.64 ± 8.16	69.51 ± 4.29
6i	46.34 ± 1.60	48.08 ± 2.16	50.78 ±5.07	58.06 ± 4.10	59.43 ± 2.12	61.06 ± 3.05
6j	36.27 ± 3.49	37.57 ± 2.03	39.90± 1.10	41.20 ± 4.06	41.70 ± 2.72	43.62 ± 1.65
6k	40.57 ± 4.65	41.94 ± 3.45	44.68 ±3.46	45.46 ± 4.00	46.64 ± 01.47	51.78 ± 3.12
6l	43.26 ± 1.64	43.63 ± 1.06	54.94 ± 2.13	56.13 ± 0.82	56.55 ± 2.09	60.15 ± 4.01
6m	48.51 ± 4.33	49.15 ± 3.12	50.73 ± 3.02	53.23 ± 4.19	53.47 ± 3.44	55.87 ± 2.23
6n	41.34 ± 3.06	44.33 ± 2.49	45.34 ± 5.05	59.69 ± 4.17	59.89 ± 1.03	63.80 ± 2.19
6o	50.26 ± 6.11	51.64 ± 3.74	55.90 ± 3.50	60.09 ± 1.01	61.81 ± 2.44	63.75 ± 4.07
6p	40.36 ± 2.75	46.72 ± 3.03	48.03 ± 4.23	54.41 ± 3.05	57.72 ± 4.97	59.84 ± 2.04
7a	35.69 ± 4.14	37.66 ± 4.81	39.19±2.26	40.76 ± 3.14	41.89 ± 5.049	42.44 ± 3.11
7b	50.18 ± 5.34	52.03 ± 2.63	52.31± 1.08	55.08 ± 3.05	56.19 ± 3.07	58.23 ± 2.04
7c	43.01 ± 2.55	43.55 ± 4.66	47.97 ± 1.04	55.14 ± 2.08	56.03 ± 2.04	54.45 ± 3.06
8a	40.59 ± 3.43	35.88 ± 1.72	42.52 ± 5.10	39.87 ± 4.47	39.75 ± 2.02	37.95 ± 3.04
Quercetin	42.34 ± 5.33	48.93 ± 4.14	56.26 ± 4.25	57.89 ± 6.35	60.62 ± 5.94	62.73 ± 1.94
Donepezil	45.66 ± 3.68	49.16 ± 3.55	57.12 ± 7.72	65.47 ± 5.16	68.91 ± 6.35	76.68 ± 5.45

[a] Cell viability was tested through the MTT assay. Data are expressed as the mean ± SEM of the three independent experiments.

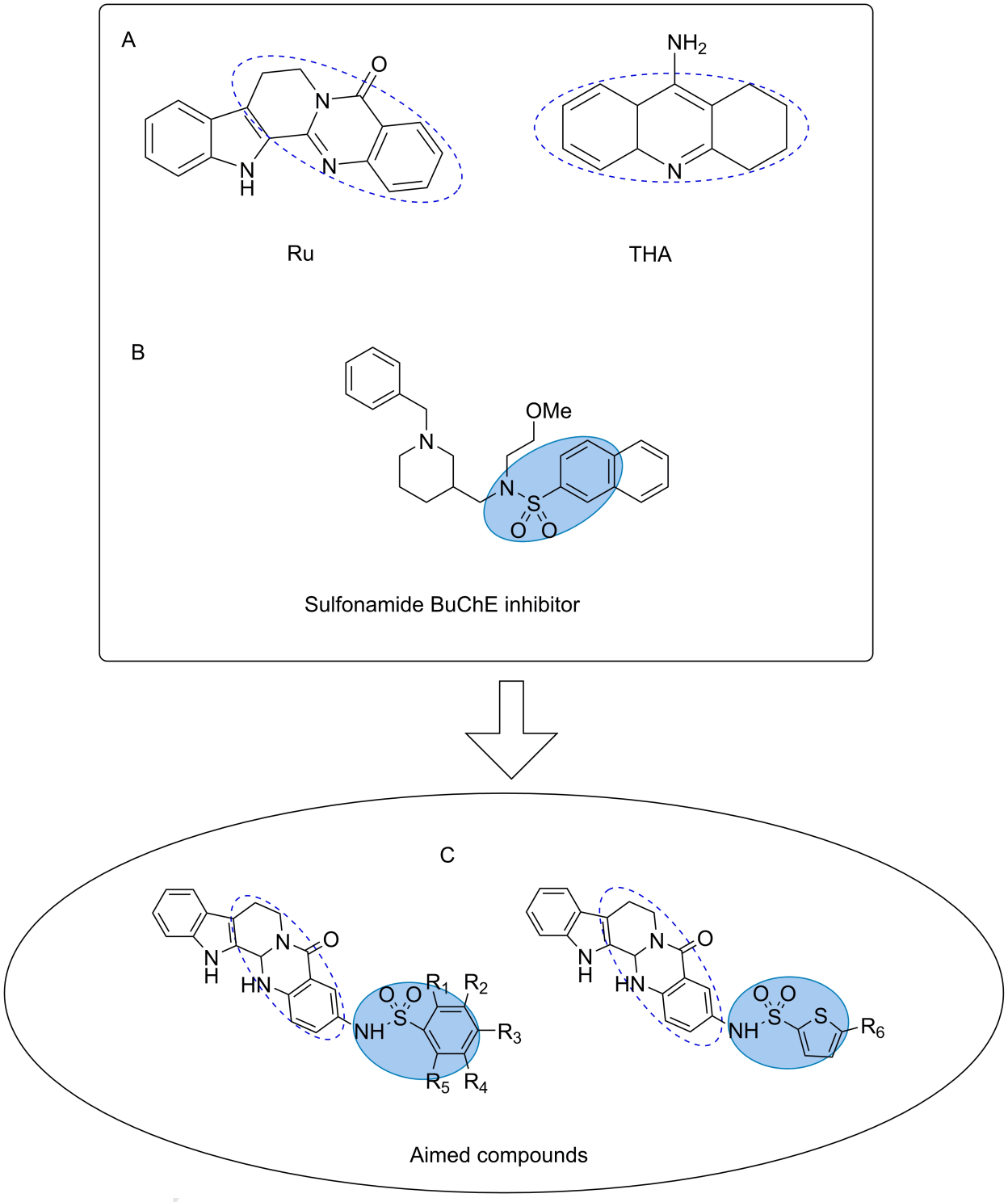
A
O
N
N
N
H
NH2
N
Ru
THA
B
OMe
N
N
S
O
O
Sulfonamide BuChE inhibitor
C
N
H
N
HN
O
NH
S
O
O
R1
R2
R3
R4
R5
R6
Aimed compounds

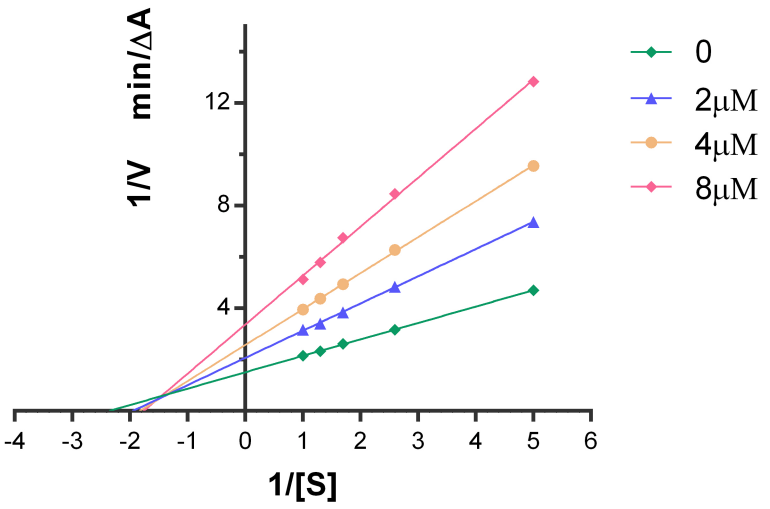

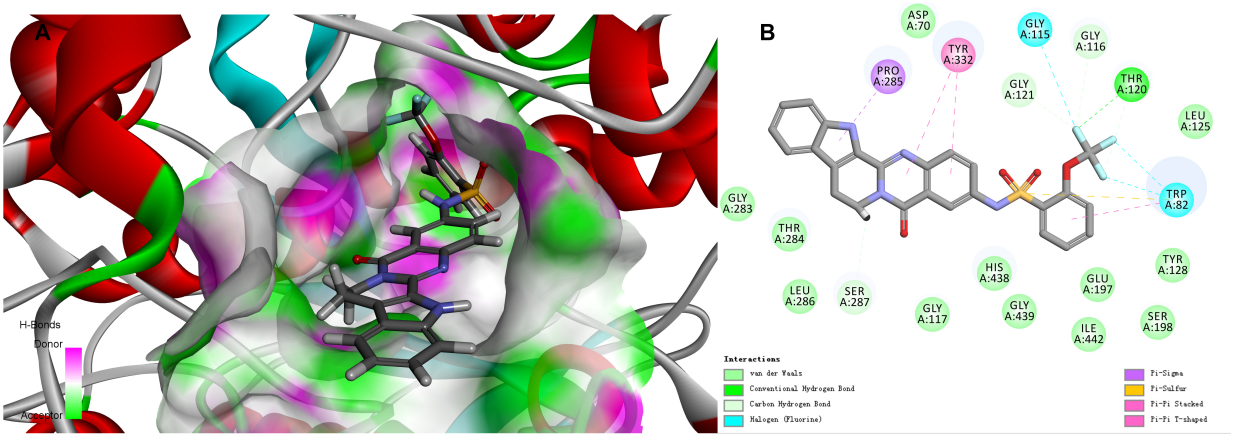

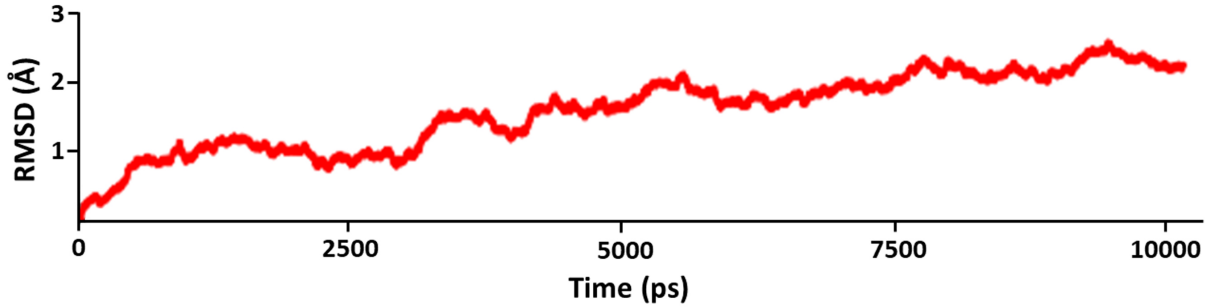

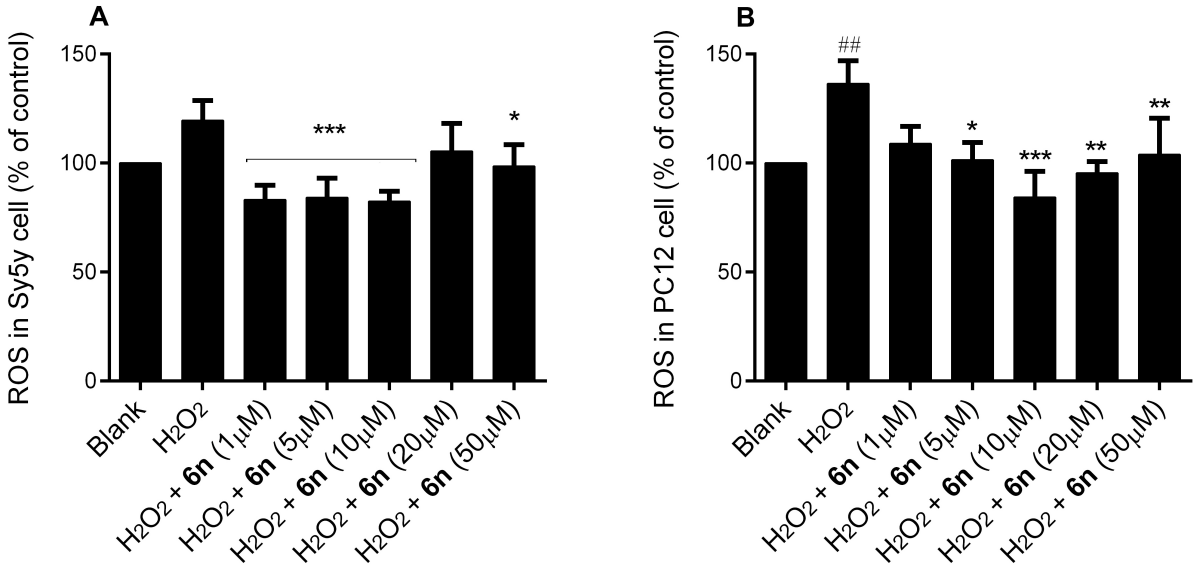

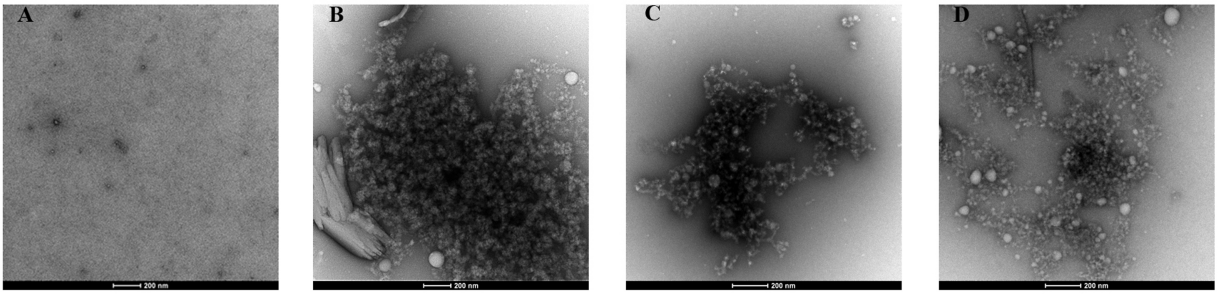

Aβ alone (0 h) Aβ alone (48 h) Aβ+**6n** (48 h) Aβ+Donepezil (48 h)

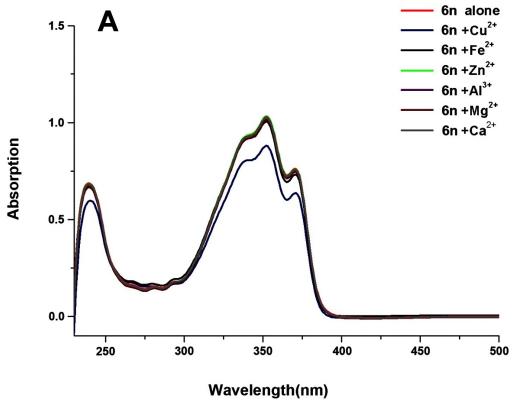

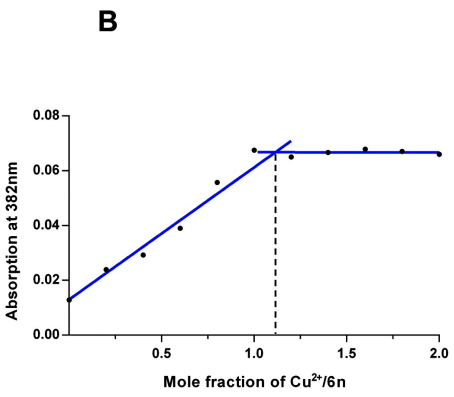

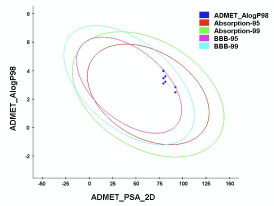

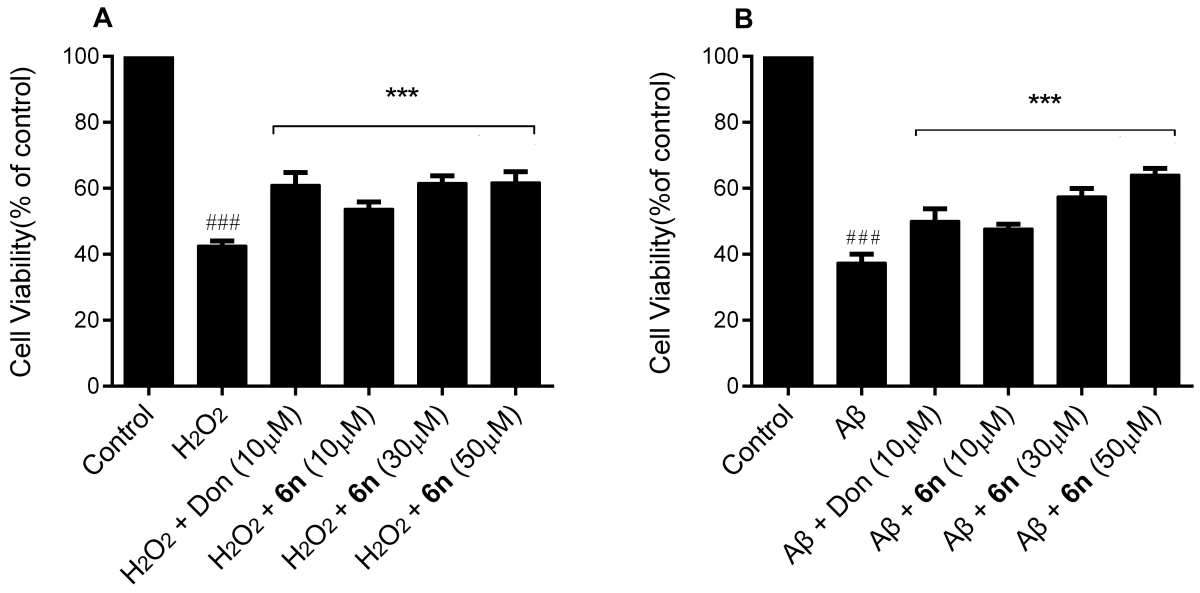

Highlights:

- A series of 3-amino-substituted rutacecarpine derivatives were synthesized in accordance with the modified Bergman synthetic procedure as MTDLs for the treatment of AD.
- Compound **6n** presented better inhibitory activity and selective effect on BuChE.
- Compound **6n** inhibited ROS formation and displayed antioxidant effects.
- Compound **6n** displayed self-mediated Aβ aggregation inhibition and selective Cu^{2+} chelating property.
- Compound **6n** had good drug-likeness and great neuroprotection.
- Compound **6n** was considered to be a promising MTDL for the treatment of AD.